Longitudinal analysis shows durable and broad immune memory after SARS-CoV-2 infection with persisting antibody responses and memory B and T cells

Kristen W. Cohen[1,*], Susanne L. Linderman[2,*], Zoe Moodie[1], Julie Czartoski[1], Lilin Lai[4,10,11], Grace Mantus[4,10], Carson Norwood[4,10], Lindsay E. Nyhoff[4,11], Venkata Viswanadh Edara[4,10,11], Katharine Floyd[4,10,11], Stephen C. De Rosa[1,7], Hasan Ahmed[8], Rachael Whaley[1], Shivan N. Patel[3], Brittany Prigmore[1], Maria P. Lemos[1], Carl W. Davis[2], Sarah Furth[1], James O'Keefe[6], Mohini P. Gharpure[2], Sivaram Gunisetty[2], Kathy A. Stephens[5], Rustom Antia[8], Veronika I. Zarnitsyna[2,9], David S. Stephens[6], Srilatha Edupuganti[3], Nadine Rouphael[3], Evan J. Anderson[4-6], Aneesh K. Mehta[6], Jens Wrammert[4,10**], Mehul S. Suthar[4,10,11**], Rafi Ahmed[2,**], and M. Juliana McElrath[1,7,**]

*Co-first authors and **Co-senior authors

Address correspondence to jmcelrat@fredhutch.org or rahmed@emory.edu

[1]Vaccine and Infectious Disease Division, Fred Hutchinson Cancer Research Center, Seattle, WA, 98109, USA

[2]Emory Vaccine Center and Department of Microbiology and Immunology, Emory University, Atlanta, GA 30322, USA

[3]Department of Medicine, Division of Infectious Diseases, Hope Clinic of Emory Vaccine Center, Emory University School of Medicine, Atlanta, GA 30329, USA

[4]Center for Childhood Infections and Vaccines of Children's Healthcare of Atlanta, Emory University Department of Pediatrics Department of Medicine, Atlanta, GA 30322, USA

23 [6]Emory University School of Medicine, Department of Medicine, Atlanta, GA 30322,
24 USA
25 [7]Departments of Laboratory Medicine and Medicine, University of Washington, Seattle,
26 WA 98195, USA
27 [8]Department of Biology, Emory University, Atlanta, GA 30322, USA
28 [9]Department of Microbiology and Immunology, Emory University, Atlanta, GA 30322,
29 USA
30 [11]Yerkes National Primate Research Center, Atlanta, GA 30329, USA
31
32 **Funding Acknowledgments:**
33 The research reported in this publication was supported in part by COVID supplements
34 from the National Institute of Allergy and Infectious Diseases and the Office of the
35 Director of the National Institutes of Health under award numbers UM1AI068618-14S1
36 and UM1AI069481-14S1 (MJM); UM1A057266-S1, U19AI057266-17S1 and
37 U19AI090023 (R. Ahmed); ORIP/OD P51OD011132 (MSS); and T32AI074492 (LEN).
38 This work was also supported by grants from the Oliver S. and Jennie R. Donaldson
39 Charitable Trust (R. Ahmed); Paul G. Allen Family Foundation Award #12931 (MJM);
40 Seattle COVID-19 Cohort Study (Fred Hutchinson Cancer Research Center, MJM); the
41 Joel D. Meyers Endowed Chair (MJM); An Emory EVPHA Synergy Fund award (MSS
42 and JW); COVID-Catalyst-I^3 Funds from the Woodruff Health Sciences Center (MSS);
43 the Center for Childhood Infections and Vaccines (MSS and JW); Children's Healthcare
44 of Atlanta (MSS and JW), a Woodruff Health Sciences Center 2020 COVID-19 CURE

Award (MSS) and the Vital Projects/Proteus funds. The content is solely the responsibility of the authors and does not necessarily represent the official views of the funders.

SUMMARY

Ending the COVID-19 pandemic will require long-lived immunity to SARS-CoV-2. We evaluated 254 COVID-19 patients longitudinally from early infection and for eight months thereafter and found a predominant broad-based immune memory response. SARS-CoV-2 spike binding and neutralizing antibodies exhibited a bi-phasic decay with an extended half-life of >200 days suggesting the generation of longer-lived plasma cells. In addition, there was a sustained IgG+ memory B cell response, which bodes well for a rapid antibody response upon virus re-exposure. Polyfunctional virus-specific CD4+ and CD8+ T cells were also generated and maintained with an estimated half-life of 200 days. Interestingly, the CD4+ T cell response equally targeted several SARS-CoV-2 proteins, whereas the CD8+ T cell response preferentially targeted the nucleoprotein, highlighting the importance of including the nucleoprotein as a potential vaccine antigen. Taken together, these results suggest that broad and effective immunity may persist long-term in recovered COVID-19 patients.

Keywords:

SARS-CoV-2, COVID-19, Immune memory, Antibody, Kinetics, Neutralization, CD4+ T cells, CD8+ T cells, B cells, Spike, RBD, Endemic coronaviruses

68 **INTRODUCTION**

69 The COVID-19 pandemic caused by the rapid spread of SARS-CoV-2, a novel
70 betacoronavirus, continues to cause significant morbidity and mortality. The induction of
71 effective early immune control of SARS-CoV-2 and durable immune memory is critical
72 to prevent severe disease and to protect upon re-exposure. SARS-CoV-2 infection
73 induces polyclonal humoral and cellular responses targeting multiple viral proteins
74 described in cross-sectional and longitudinal studies (Sette and Crotty, 2021). More
75 comprehensive, quantitative analyses with extensive serial sampling in larger numbers
76 of COVID-19 patients are limited, and could resolve some conflicting views about the
77 durability of humoral immunity. Importantly, defining the frequency, immune function
78 and specificity of the antibodies, memory B and T cell responses among COVID-19
79 patients, and identifying when they appear and how long they persist can provide
80 understanding of the integral components for long-lived immunity to SARS-CoV-2 and
81 potentially other human coronaviruses that emerge in the future (Stephens and
82 McElrath, 2020).

83 We initiated two prospective COVID-19 patient cohorts in Seattle and Atlanta during
84 the first surge of the pandemic to investigate long-term immunity to SARS-CoV-2.
85 Among 254 COVID-19 patients enrolled and frequently sampled, we identify binding
86 and neutralizing antibodies to SARS-CoV-2 as well as antigen-specific B and T cells
87 elicited early after infection, define their specificities, quantify the extent of antibody
88 boosting of cross-reactive responses to other coronaviruses, and further characterize
89 the decay rate and durability of these immune parameters over 250 days. We employ

90 highly standardized or validated assays that are also being used to evaluate immunity in
91 recent and ongoing clinical vaccine trials (Anderson et al., 2020; Doria-Rose et al.,
92 2021; Sadoff et al., 2021). This indepth longitudinal study demonstrates that durable
93 immune memory persists in most COVID-19 patients, including those with mild disease,
94 and serves as a framework to define and predict long-lived immunity to SARS-CoV-2
95 after natural infection. This investigation will also serve as a benchmark for immune
96 memory induced in humans by SARS-CoV-2 vaccines.
97

98 # RESULTS

99 **COVID-19 study population**

100 COVID-19-confirmed patients were recruited into our longitudinal study of SARS-
101 CoV-2 specific B and T cell memory after infection. A total of 254 patients enrolled at
102 two sites, Atlanta and Seattle, starting in April 2020 and returned for follow up visits over
103 a period of 250 days. We were able to collect blood samples at 2-3 time points from 165
104 patients and at 4-7 time points from another 80 patients, which allowed us to perform a
105 longitudinal analysis of SARS-CoV-2-specific B and T cell responses on a large number
106 of infected patients. The demographics and baseline characteristics of this cohort are
107 described in Table S1. The study group was 55% female and 45% male and between
108 18-82 years old (median, 48.5 years). Based on World Health Organization (WHO)
109 guidelines of disease severity, 71% of study participants exhibited mild disease, 24%
110 had moderate disease, and 5% experienced severe disease.

111 **Antibody responses to SARS-CoV-2 spike protein show a bi-phasic decay with an**
112 **extended half-life**

113 Binding antibodies to the SARS-CoV-2 full length spike protein, to the receptor
114 binding domain (RBD) and to the N terminal domain (NTD) of the spike protein were
115 assessed in COVID-19 patients (n=222) over a period of 8 months post symptom onset.
116 We included healthy individuals age 18-42 years as negative controls whose
117 longitudinal blood samples were collected before the emergence of the COVID-19
118 pandemic. These pre-pandemic samples (n=51) were from recipients of either the
119 seasonal inactivated influenza vaccine (n=27, collected from 2014-2018) or the live
120 yellow fever virus (YFV-17D) vaccine (n=24, collected from 2005-2007). The Mesoscale
121 multiplex assay was used to measure IgG, IgA, and IgM antibody responses to SARS-
122 CoV-2 proteins in the COVID-19 patients and in the pre-pandemic healthy controls.

123 The magnitude of serum IgG antibodies binding to the SARS-CoV-2 spike protein
124 increased in 92% of COVID-19 convalescent participants (n=222) relative to pre-
125 pandemic controls (Figure 1A). The IgG responses to SARS-CoV-2 spike, RBD, and
126 NTD declined over time with half-lives of 126 (95% confidence interval [95%CI] [107,
127 154]), 116 (95%CI [97, 144]), and 130 (95%CI [110, 158]) days, respectively, as
128 estimated by an exponential decay model (Figure 1A-C and S1A). We also estimated
129 antibody waning using a power law model, which models a scenario in which the rate of
130 antibody decay slows over time. The power law model produced a better fit for the
131 decay of the SARS-CoV-2 spike, RBD, and NTD binding IgG antibodies (ΔAICs>10),
132 suggesting that spike-specific antibodies plateau over time. Because the decay rate

133 changes over time, the half-life is predicted to change over time as well; therefore, we
134 used the power law model to estimate the half-lives at 120 days after symptom onset.
135 The power law estimated half-lives for the IgG antibody responses to spike ($t_{1/2}$=238
136 days), RBD ($t_{1/2}$=209 days), and NTD ($t_{1/2}$=244 days) were longer than those estimated
137 by the exponential decay model (Figure S1A, C), indicating that the concentration of
138 these IgG antibodies may be starting to stabilize. IgA (Figure 1D-F) and IgM (Figure 1G-
139 I) antibodies reactive to the SARS-CoV-2 spike also increased after SARS-CoV-2
140 infection but were detected at lower levels and declined faster than the SARS-CoV-2-
141 reactive IgG antibodies. As expected, spike-binding IgM decayed more rapidly than
142 spike-binding IgA and IgG. Taken together these results show that antibody responses,
143 especially IgG antibody, were not only durable in the vast majority of patients in the 250
144 day period but also that the bi-phasic decay curve suggests the generation of longer
145 lived plasma cells producing antibody to the SARS-CoV-2 spike protein.
146 We also examined the antibody response to the SARS-CoV-2 nucleocapsid protein
147 in these infected patients. As expected, the COVID-19 patients showed higher levels of
148 antibody to the nucleocapsid protein compared to the pre-pandemic healthy controls
149 (Figure S2). However, the nucleocapsid-specific antibodies declined with a much
150 shorter half-life of 63 days (95%CI [58, 70]) compared to the spike protein antibodies
151 (Figure S1A, C). Also, the nucleocapsid reactive IgG decay rate was best fit by the
152 exponential model and not the power law model in contrast to what we observed with
153 the spike IgG antibody decay rate (Figure S1A). Thus, the nucleocapsid reactive IgG
154 not only declined much faster but also showed less evidence of stabilizing antibody

levels consistent with a response driven disproportionately by short-lived antibody secreting cells – at least at this stage of the immune response.

Stable and long-lived antibody responses to common human alpha- and betacoronaviruses in pre-pandemic healthy controls

We were interested in determining if SARS-CoV-2 infection had any effect on the levels of antibody to the circulating human alpha- and betacoronaviruses. As a prelude to this question, we first examined antibody levels to the spike protein of the two circulating alphacoronaviruses (229E and NL63) and the two betacoronaviruses (HKU1 and OC43) in our pre-pandemic samples. As shown in Figure 2, all 51 pre-pandemic samples had clearly detectable levels of IgG and IgA antibodies to the spike proteins of the four human coronaviruses. This is the expected result since seropositivity to these coronaviruses is very high in the adult population. But what was quite interesting was the remarkable stability of these antibody responses over a 200-day period in the pre-pandemic serum samples (shown as red lines in Figure 2). These were essentially flat lines with no decline in the antibody levels and question the prevailing belief that antibody responses to the endemic coronaviruses are short-lived (Callow et al., 1990; Edridge et al., 2020; Lavine et al., 2021). While some occasional boosting of these childhood-acquired coronavirus infections cannot be ruled out, these data showing such stable antibody titers are best explained by the persistence of long-lived plasma cells in the bone marrow many years after infection (Amanna et al., 2007; Davis et al., 2020; Hammarlund et al., 2003; Manz et al., 1997; Slifka et al., 1998).

177

178 **COVID-19 infection results in increased levels of antibodies to two common**

179 **human betacoronaviruses (HKU1 and OC43) and to SARS-CoV-1**

180 We next examined if SARS-CoV-2 infection had any impact on the levels of

181 antibodies to the other human coronaviruses. We measured IgG, IgA, and IgM antibody

182 binding to the spike proteins of other known human coronaviruses in the COVID-19

183 patients (n=222 for IgG and n=190 for IgA and IgM) and compared these data to the 51

184 pre-pandemic healthy donor samples. In the COVID-19 patients, IgG and IgA antibodies

185 to the alphacoronaviruses, 229E and NL63, did not show any significant changes

186 compared to the antibody levels in the pre-pandemic healthy controls (Figure 2A, B, F,

187 G; Figure S1C, D). In contrast, the IgG and IgA antibodies to betacoronaviruses HKU1

188 and OC43 were substantially elevated in COVID-19 patients relative to pre-pandemic

189 controls (Figure 2C, D, H, I; Figure S1C, D; $p<0.0001$). After this boost, HKU1 and

190 OC43 IgG antibody levels declined with estimated half-lives of 288 (95%CI [235, 372])

191 and 212 (95%CI [176, 268]) days, respectively (exponential decay model). IgM levels to

192 common betacoronaviruses HKU1 and OC43 were low in both pre-pandemic controls

193 and COVID-19 patients (Figure 2M, N). While pre-existing exposure and antibodies

194 against HKU1 and OC43 betacoronaviruses are common in adults, pre-existing SARS-

195 CoV-1 exposure is rare and antibody levels to SARS-CoV-1 spike protein were very low

196 (essentially negative) in the pre-pandemic healthy controls. However, SARS-CoV-1

197 spike-reactive antibodies increased significantly after SARS-CoV-2 infection. These

198 increases were quite striking for IgG ($p=0.0038$) and also IgA ($p=0.0084$) and most likely

199 represent cross-reactive antibodies directed to SARS-CoV-2 spike epitopes that are
200 conserved between SARS-CoV-2 and SARS CoV-1 (Ellis et al., 2021). These newly
201 induced cross-reactive IgG antibodies generated after COVID-19 infection declined with
202 an estimated half-life of 215 days (95%CI [168, 298]) (exponential decay model) (Figure
203 2). Taken together, these results show that people infected with SARS-CoV-2 may have
204 also have some heightened immunity against the common human betacoronaviruses
205 and more importantly against SARS-CoV-1.
206
207 **Durable neutralizing antibody responses to SARS-CoV-2 in infected patients**
208 Neutralizing antibodies were measured with a live virus focus reduction
209 neutralization test that uses a recombinant SARS-CoV-2 virus expressing the
210 fluorescent reporter gene mNeonGreen (FRNT-mNG) (Figure 3A). During the first 250
211 days post-symptom onset, $FRNT_{50}$ titers varied considerably between individuals and
212 ranged from <20 to 3726 (Figure 3A). Of the 183 individuals for whom longitudinal
213 neutralization titers were assayed, 140 (77%) had at least one timepoint with
214 neutralization titers above the limit of detection (>20). Seventy-five percent (43/57) of
215 COVID-19 patients generated serum neutralizing antibodies between 30 – 50 days after
216 symptom onset, and similarly 72% (48/67) had measurable titers between 180 – 263
217 days after symptom onset. Using an exponential decay model, we evaluated the
218 kinetics of neutralizing antibody titers after day 42 and estimated a half-life of 150 days
219 (95%CI [124, 226]). However, similar to the spike reactive IgG binding antibodies, we
220 hypothesized that the neutralizing antibody rate of decay may actually slow over time

221 during the recovery period. To address this, we fit a power law to the data. The power
222 law model fit significantly better than the exponential decay model (ΔAIC=9) and
223 estimated the half-life of neutralizing antibody responses at 120 days post-symptom
224 onset to be 254 days (95%CI [183, 400]).
225 Next, we assessed the relationship between the levels of spike and RBD binding
226 antibodies and SARS-CoV-2 neutralization. Figures 3B and C show the SARS-CoV-2
227 spike and RBD binding antibody response kinetics of the 183 participants for whom
228 neutralization titers were assessed. These exhibited a wide range of antibody binding
229 levels ranging from non-responders (n=11) who did not elicit antibody titers above those
230 of pre-pandemic controls (defined as a COVID-19 patient titer below the mean pre-
231 pandemic antibody titer plus 3 standard deviations, see dashed line on Figure 3B, C) to
232 those with IgG levels >200,000 AU/ml. Spike and RBD binding IgG levels correlated
233 significantly with the neutralization titers (Figure 3D, E; $p<0.0001$).
234 Taken together, our findings show that induction of neutralizing antibodies occurs in
235 the majority of COVID-19 patients. These neutralizing antibodies can persist over the 8-
236 9 month period following infection, and show a correlation with spike and RBD binding
237 IgG.
238
239 **SARS-CoV-2 spike and RBD-specific memory B cells increase for several months**
240 **after infection and then plateau over 8 months**
241 Memory B cells (MBC) are an important component of humoral immunity and
242 contribute to viral control by generating antibody responses upon re-exposure to the

243 pathogen. We used full-length spike and RBD antigen probes to quantify the
244 frequencies of SARS-CoV-2 spike- and RBD-specific MBC in longitudinal PBMC
245 samples from 111 COVID-19 patients (Figure 4) and from 29 pre-pandemic controls
246 (Figure S3A, B). Our flow cytometric gating strategy to identify SARS-CoV-2 specific
247 MBC and classify them as IgG, IgM and IgA MBC isotypes is shown in Figure 4A.
248 Among the total MBC, the spike IgG+ MBCs were significantly increased in COVID-
249 19 patients (n=111; Figure 4B) in comparison to pre-pandemic controls (n=29; Figure
250 S3A) (median increase, 0.73% vs. 0.02%; $p<0.0001$). After a steep early expansion
251 over the first 2-3 months, the spike IgG+ MBC persisted in COVID-19 patients with no
252 decline out to 250 days post symptom onset. These findings (Figure 4B) are supported
253 by a positive slope (0.004) from the model of the longitudinal spike IgG+ MBC
254 responses after day 30 (95%CI [0.002, 0.006], $p<0.001$; Figures S4A, B).
255 The spike IgM+ MBC appeared within the first two weeks post-symptom onset and
256 quickly declined (Figure 4C, D). The decay continued after day 30 (slope=-0.007,
257 95%CI [-0.010, -0.005], $p<0.001$). One month after symptom onset, 56% of spike MBC
258 were IgG+, which increased to a peak of 80% at 5-6 months (Figure 4D). Circulating
259 spike IgA+ MBC were also detectable in many subjects at low frequencies and without
260 significant change over time (day 30 to 250: slope=0.000, 95%CI [-0.002, 0.002],
261 $p=0.91$, Figure 4D).
262 Since the RBD contains the primary neutralizing epitopes on the spike, we also
263 used an RBD-specific probe to characterize this subset of spike-specific memory B
264 cells. Overall, approximately 20% of the spike IgG+ memory B cells targeted the RBD,

265 which was consistent across subjects and time (Figure 4E, F). As expected, RBD+ IgM+
266 MBC emerged early in infection and subsequently switched to RBD+ IgG+ MBCs, which
267 gradually increased during follow-up (day 30 to 250: slope=0.004, 95%CI [0.002, 0.005],
268 p<0.001, Figure 4E). Thus, the maintenance of circulating spike- and RBD-specific IgG
269 memory B cells suggests that these cells could be recruited for a rapid secondary
270 response following re-exposure or after vaccination.
271
272 **Induction of durable and polyfunctional virus specific memory CD4+ and CD8+ T**
273 **cells in infected patients**
274 CD4+ T cells are critical for generation of high affinity antibody responses and can
275 also have anti-viral effects. In addition, they provide help for CD8+ T cell responses,
276 which are vital for killing infected cells and mediating viral clearance. Thus, we next
277 examined virus-specific CD4+ and CD8+ T cell responses longitudinally in COVID-19
278 patients and uninfected controls using a high-dimensional, multi-parameter *ex vivo*
279 intracellular cytokine staining (ICS) assay. The assay is sensitive, precise and specific
280 for detection of antigen-specific T cells expressing multiple cytokines and effector
281 molecules following a short-term (6 hours) stimulation with peptide pools. Our lab
282 developed and validated the assay, and we are currently using the method to quantitate
283 Th1/Th2 CD4+ and CD8+ T cell responses in SARS-CoV-2 vaccine trials. Here, we
284 assessed T cell responses to the SARS-CoV-2 structural (S, E, M and N) and
285 accessory proteins (ORF 3a, 6, 7a, 7b, and 8) using overlapping peptide pools that
286 span the sequences of these proteins.

287 Among COVID-19 patients, 89% (102/113) mounted CD4+ T cell responses (Figure
288 5A) recognizing at least one SARS-CoV-2 structural protein that was detectable at one
289 or more visits. By contrast, SARS-CoV-2 specific CD4+ T cells were rarely detected in
290 the uninfected control group using this assay (Figure S3C). Antigen-specific CD4+ T
291 cells expanded over the first month after infection and then gradually declined over
292 subsequent months. Their estimated half-life was 207 days (95%CI [104, 211]) as
293 shown in Figure 5A, and these findings are supported by the individual CD4+ T cell
294 response levels and slopes after day 30 (slope= -0.0033, 95%CI [-0.0017, -0.0066],
295 $p<0.0001$) (Figure S4C, D). Of note, we observed a wide range in the total magnitude of
296 responses, some reaching >1% of circulating CD4+ T cells, and an overall median
297 frequency of 0.51% (Figures 5A and S5).
298 To better characterize the development of T cell memory in SARS-CoV-2 infection,
299 we examined the differentiation profiles of virus-specific T cells longitudinally in COVID-
300 19 patients. Based on CD45RA and CCR7 expression, SARS-CoV-2-specific CD4+ T
301 cells were primarily central memory phenotype (CD45RA- CCR7+) and to a lesser
302 extent effector memory (CCRA-CCR7-); this profile of the memory T cell subsets was
303 very consistent between subjects and stable over time (Figure 5B). The antigen-specific
304 CD4+ T cells were Th1-biased with a predominant CXCR3+CCR6- phenotype, and
305 highly polyfunctional, with simultaneous detection of antigen-specific CD154, IFN-γ, IL-
306 2, TNF-α and less frequently granzyme B in the early expansion phase (21-60 days post
307 symptom onset; median, 30 days) (Figure 5C). Interestingly, many of the virus-specific
308 CD4+ T cells also exhibited this polyfunctionality at the memory time point (>180 days

309 post symptom onset; median, 203 days) (Figure 5D). Circulating SARS-CoV-2-specific
310 Th2 (IL-4, IL-5 and IL-13), Th17 (IL-17) or perforin-expressing subsets were not
311 detected (Figure 5C and D).

312 Next, we examined the CD8+ T cell responses in COVID-19 patients and found that
313 69% generated CD8+ T cells recognizing at least one SARS-CoV-2 structural protein
314 that were detectable at one or more visits (Figure 6A), in contrast to infrequent to rare,
315 low-level antigen specific responses in the uninfected control donors (Figure S3D).
316 Expansion of CD8+ T cells occurred over the first month and then frequencies gradually
317 declined, with a half-life of 196 days (95%CI [92, 417]) and a negative estimated slope
318 after 30 days of symptom onset (slope=-0.004, 95%CI [-0.002, -0.008], $p<0.0001$)
319 (Figure 6A). The median frequency of SARS-CoV-2-specific CD8+ T cells was 0.2%,
320 indicating a lower overall response magnitude than observed for CD4+ T cells.
321 However, like the CD4+ T cells, a wide range in magnitudes was observed with many
322 SARS-CoV-2-specific CD8+ T cell frequencies above 1% and even up to 12% (Figure
323 6A).

324 A very different pattern of phenotypic changes were observed with virus-specific
325 CD8+ T cells compared to what we saw with the CD4+ T cells (Figure 6B vs. Figure
326 Figure 5B). In contrast to the dominance of the central memory subset with SARS-CoV-
327 2-specific CD4+ T cells, the vast majority of the virus-specific CD8+ T cells showed an
328 effector memory phenotype during the early phase of the response. However, this
329 population of SARS-CoV-2-specific effector memory (CD45RA-CCR7-) contracted over
330 time (slope=-0.904, $p<0.0001$; Figure 6B) and simultaneously there was an increase in

331 the proportion of the TEMRA (CD45RA+CCR7-) subset of virus-specific CD8+ T cells
332 (slope=0.075, p<0.0001; Figure 6B). A small but stable fraction of SARS-CoV-2-specific
333 CD8+ T cells expressed a central memory phenotype (slope=0.024, p=ns; Figure 6B).
334 The SARS-CoV-2-specific CD8+ T cells were highly polyfunctional with the highest
335 magnitude populations secreting IFN-γ, TNF-α and granzyme B; other dominant
336 subsets also expressed IL-2 or perforin (Figure 6C, D). This polyfunctional profile was
337 seen in the expansion phase (median 30 days; Figure 6C) and also at the later time
338 points (>180 days post symptom onset; median 203 days; Figure 6D). It is important to
339 note that this pattern of CD8+ T cell differentiation has been described in detail after
340 vaccination in humans with the live attenuated yellow fever virus vaccine (YFV-17D)
341 (Akondy et al., 2017). This YFV-17D vaccine generates long-lived and functional virus
342 specific memory CD8+ T cells that persist in humans for decades (Akondy et al., 2017;
343 Veit et al., 2018). That the CD8+ T cell differentiation program after COVID-19 infection
344 resembles what is seen after YFV infection of human suggests that COVID-19 patients
345 may also generate long-lived CD8+ T cell memory.
346
347 **CD4+ and CD8+ cells target different SARS-CoV-2 antigen specificities**
348 The majority of COVID-19 patients generated CD4+ T cells that recognized most
349 SARS-CoV-2 viral structural and accessory proteins, with the highest percentage
350 responding to S2 (78%) and S1 (69%) (Figure 5E, F). Among the COVID-19 subjects
351 with positive responses, the proportion of SARS-CoV-2-specific CD4+ T cells reacting to

352 each peptide pool was evenly distributed (Figure 5F). Thus, CD4+ T cells equally
353 targeted multiple SARS-CoV-2 proteins.
354 In contrast to the results seen with CD4+ T cells, SARS-CoV-2-specific CD8+ T
355 cells showed preferential recognition of the nucleocapsid protein. The dominant CD8+ T
356 cell response rate was directed to the nucleocapsid (57%), followed by ORFs 7a, 7b,
357 and/or 8 (25%), S1 (25%), ORFs 3a and/or 6 (16%), S2 (12%) and E and/or M (9%)
358 (Figure 6E). Also, among the COVID-19 patients with CD8+ T cell responses, there was
359 a bias with the largest percentage (median, 43%) reacting to the nucleoprocapsid
360 protein (Figure 6F). While SARS-CoV-2 CD8+ T cell responses rates were much lower
361 in uninfected controls, when present in a few control donors with lower frequencies,
362 these were also targeted to the nucleocapsid protein (Figure S3D). A likely explanation
363 for these findings is that in SARS-CoV-2 infection, antigen-presenting cells *in vivo* may
364 display a higher proportion of peptides derived from the nucleocapsid protein and hence
365 more nucleocapsid-specific CD8+ T cells are generated during infection. This has
366 interesting implications suggesting that nucleocapsid-specific CD8+ T cells might be
367 more efficient in recognizing virally infected cells.
368
369 **Age and disease severity are significantly associated with magnitude of SARS-**
370 **CoV-2 immune responses**
371 We evaluated whether COVID-19 patient age, disease severity, or sex could
372 account in part for the heterogeneity observed among the SARS-CoV-2-specific
373 immune responses as estimated from the individual models (post day 30 for cellular and

374 post day 42 for antibody responses). We observed that age was significantly associated
375 with higher immune responses to SARS-CoV-2, independently of any covariation with
376 disease severity (Figure 7A). Neutralizing antibody titers and IgG antibody responses to
377 nucleocapsid increased 1.35-fold and 1.25-fold, respectively, with each decade of age
378 and the same disease severity (95%CIs [1.19, 1.54] and [1.08, 1.43], p values<0.003).
379 Similarly, increased age positively correlated with increased frequencies of spike and
380 RBD-specific IgG+ memory B cells, with 1.19 to 1.24-fold higher responses per decade
381 of age (p values<0.02; Figure 7A), accounting for disease severity. Increased age also
382 correlated with higher SARS-CoV-2 and S1-specific CD4+ T cell responses (1.16-1.20-
383 fold increase by decade of age, p values<0.02) and N-specific CD8+ T cell responses
384 (1.24-fold increase by decade of age, p=0.039) accounting for disease severity (Figure
385 7A).

386 Since the cohort included primarily persons with mild to moderate COVID-19, we
387 had limited ability to assess the relationship of severe disease and SARS-CoV-2
388 immune responses, especially among the cellular responses. However, we found that
389 after accounting for age, severe disease (WHO score >4) was associated with higher
390 IgG antibodies to nucleocapsid, spike, RBD, and NTD (Figure 7B, C), and SARS-CoV-2
391 neutralization titers (Figure 7D). Severe disease was also associated with 2.30 to 2.46-
392 fold higher S1, E and/or M, and nucleocapsid-specific CD4+ T cells (all p values<0.05;
393 Figure 7B). We found no significant relationships between sex and the immune
394 responses evaluated, apart from 1.66-fold higher IgG NTD responses antibodies among
395 males compared to females, after accounting for age and disease severity (95%CI

396 [1.08, 2.55], p=0.022). In all, our analyses suggest that there are synergistic, but also
397 independent mechanisms driving higher adaptive immune responses in COVID-19
398 patients who are older and/or who experienced more severe disease.
399
400 **Early SARS-CoV-2 B and T cell responses correlated with durable spike and RBD**
401 **IgG antibody binding and neutralization titers**
402 We assessed correlations between SARS-CoV-2-specific immune responses using
403 the individual-level models to interpolate the magnitude of responses for each COVID-
404 19 patient at early (day 30) or later (day 180) convalescent time points (Figure 7E). We
405 found that durable serum neutralization titers correlated with the magnitude of IgG+
406 binding antibodies to spike, NTD and RBD at day 180 each (day 180; Spearman
407 R=0.62, 0.61, and 0.61, respectively; all p values<0.0001). Similarly, the frequency of
408 RBD+ IgG+ memory B cells at day 30 correlated with the maintenance of RBD+ IgG
409 antibodies (day 180; Spearman R=0.53, p<0.0001) and neutralization antibody titers
410 (day 180; Spearman R=0.48, p<0.0001). We also observed that the magnitude of S1-
411 specific CD4+ T cells at day 30 correlated with durable IgG antibodies against spike
412 (day 180; Spearman R=0.56, p<0.0001), NTD (Spearman R=0.62, p<0.0001), and RBD
413 (Spearman R=0.47, p=0.0002) (Figure 7E). These findings are consistent with early
414 SARS-CoV-2 memory B cells and CD4+ T cells supporting the generation of durable
415 antibody responses.
416
417 **DISCUSSION**

418 Establishing immune memory is essential in the defense against SARS-CoV-2
419 infection. To end the COVID-19 pandemic, it is critical to know how long immunity
420 against SARS-CoV-2 will persist after infection and whether it will be sufficient to
421 prevent new infections and severe disease in years to come. Identifying in depth the
422 adaptive immune components leading to recovery and modeling the trends of each
423 response was enabled by the longitudinal sampling of a large number of COVID-19
424 patients. Here, we show that most convalescent COVID-19 patients mount durable
425 antibody, B and T cells specific for SARS-CoV-2 up to 250 days, and the kinetics of
426 these responses provide an early indication for a favorable course ahead to achieve
427 long-lived immunity. Because the cohort will be followed for 2-3 more years, we can
428 build on these results to define the progression to long-lived immunity against this novel
429 human coronavirus, which can guide rational responses when future outbreaks occur.
430 The hallmark of the initial immune defense against SARS-CoV-2 is the emergence
431 of antibodies recognizing the SARS-CoV-2 spike protein, including the RBD and NTD
432 components of the S1 subunit, during the early phase of viral replication. These
433 antibodies are likely secreted from plasmablasts rapidly generated from B cells that are
434 activated upon their first encounter with the pathogen spike antigen. The brisk rise over
435 the first month of infection, followed by a fast decline of the circulating spike IgG and IgA
436 antibodies, is a consistent finding and likely explained by the disappearance of the
437 short-lived plasmablasts. These events occur even sooner for the spike IgM and
438 nucleocapsid antibodies.

439 Some antibodies that bind to specific epitopes on the spike RBD and NTD can block
440 SARS-CoV-2 infection of respiratory epithelial cells by inhibiting the interactions of the
441 viral spike with the ACE2 receptor (Ju et al., 2020; Seydoux et al., 2020; Walls et al.,
442 2020; Zost et al., 2020). Thus, as expected, the early rise and decline of antibodies
443 neutralizing live SARS-CoV-2 were similar to the kinetics of antibodies binding the spike
444 and RBD protein. The striking finding is the bi-phasic curve of the spike-specific binding
445 and neutralizing antibody responses when analyzed with the power law model, which
446 provides a better fit for the antibody kinetics after the peak response (Zarnitsyna et al.,
447 2021). With sampling data extended to 250 days, we were able to detect a slowing of
448 the decay of these functional antibodies toward a plateau level, suggestive of the
449 generation of longer-lived plasma cells, and durable antibody responses. The
450 importance of these observations is that following recovery, neutralizing antibodies may
451 persist, albeit at low levels, and may act as the first line of defense against future
452 encounters of SARS-CoV-2 and possibly related human coronaviruses.
453 Another interesting finding of this investigation is the remarkably stable antibody
454 responses among the pre-pandemic and COVID-19 patients to the common human
455 coronaviruses that are acquired in children and adults. These data are most consistent
456 with the generation of long-lived plasma cells and refute the current notion that these
457 antibody responses to human coronaviruses are short-lived. Moreover, the COVID-19
458 patients mounted increased IgG antibody responses to SARS-CoV-1, a related
459 pathogen that none likely had experienced previous exposure. This finding is consistent
460 with the booster response of SARS-CoV-1 neutralizing antibodies that we recently

461 observed following SARS-CoV-2 mRNA vaccination (Doria-Rose et al., 2021;
462 Stamatatos et al., 2021). Taken together, these results may have implications for a
463 broader strategy for vaccines targeting multiple betacoronaviruses.
464 The durable antibody responses in the COVID-19 recovery period are further
465 substantiated by the ongoing rise in both the spike and RBD memory B cell responses
466 after over 3-5 months before entering a plateau phase over 6-8 months. Persistence of
467 RBD memory B cell has been noted (Dan et al., 2021; Gaebler et al., 2021; Rodda et
468 al., 2021). We presume this may be explained by sustained production of memory B
469 cells in germinal centers of lymph nodes draining the respiratory tract in the early
470 months, followed by the memory B cell redistribution into the circulation as the germinal
471 centers begin to recede. Thus, the induction and maintenance of memory B cells and,
472 over time, long-lived plasma cells, will continue to furnish higher affinity antibodies if re-
473 exposures occur.
474 In contrast to spike memory B cell kinetics, SARS-CoV-2-specific CD4+ and CD8+
475 memory T cells each peak early, within the first month, but then slowly decline over the
476 next 6-7 months. Central memory Th1-type CD4+ T cells dominate throughout the early
477 infection and recovery period. However, the CD8+ T cells exhibit a predominant
478 effector memory phenotype early that transitions to those effector memory cells re-
479 expressing CD45RA, maintaining expression of antiviral cytokines and effector functions
480 which have been shown to provide protective immunity against other viral pathogens.
481 We also provide clear evidence that the CD4+ T cells mount a broader antigen-specific
482 response across the structural and accessory gene products, whereas the CD8+ T cells

483 are predominantly nucleocapsid specific and spike-specific responses are substantially
484 lower in frequency.

485 Our study demonstrates the considerable immune heterogeneity in the generation
486 of potentially protective response against SARS-CoV-2, and by focusing on the
487 dynamics and maintenance of B and T cell memory responses, we were able to identify
488 features of these early cellular responses that can forecast the durability of a potentially
489 effective antibody response. The ability to mount higher frequencies of RBD-specific
490 memory IgG+ B cells early in infection was the best indicator for a durable RBD-specific
491 IgG antibody and neutralizing antibody response. In addition, higher frequency CD4+ T
492 cells were associated with stronger spike IgG and neutralizing antibody responses.
493 However, the induction and peak response of SARS-CoV-2-specific CD8+ T cells
494 occurs independently to these antibody responses. Interestingly, while it has been
495 widely reported that age correlates with COVID-19 disease severity, we found that age
496 and disease severity were independent co-variates associated with the magnitude of
497 both SARS-CoV-2-specific CD4+ T cell and humoral SARS-CoV-2 immunity, but not
498 with the magnitude of CD8+ T cell responses. In the case of T cells, whether the T cell
499 differences are related to the frequencies or specificities of pre-existing coronavirus
500 CD4+ and CD8+ T cell immunity will require additional future analysis.

501 The COVID-19 pandemic remains a global public health threat after one year of
502 overwhelming disruption and loss. Overcoming the challenges to end the pandemic is
503 accentuated by the recognition that SARS-CoV-2 can undergo rapid antigenic variation
504 that may lower vaccine effectiveness in preventing new cases and progression to

505 severe disease (Edara et al., 2021; Mascola et al., 2021; Stamatatos et al., 2021). Our findings
506 show that most COVID-19 patients induce a wide-ranging immune defense against
507 SARS-CoV-2 infection, encompassing antibodies and memory B cells recognizing both
508 the RBD and other regions of the spike, broadly-specific and polyfunctional CD4+ T
509 cells, and polyfunctional CD8+ T cells. The immune response to natural infection is
510 highly likely to provide protective immunity even against the SARS-CoV-2 variants
511 because the CD4+ and CD8+ T cell epitopes will be conserved. Thus, recovered
512 COVID-19 patients are likely to better defend against the variants than persons who
513 have not been infected but have been immunized with spike-containing vaccines only.
514 Nevertheless, vaccine induction of CD8+ T cells to more conserved antigens such as
515 the nucleocapsid, rather than just to SARS-CoV-2 spike antigens, may add benefit to
516 more rapid containment of infection as SARS-CoV-2 variants overtake the prevailing
517 strains.
518
519 **ACKNOWLEDGMENTS**
520 First, we thank the participants for volunteering their time and effort to participate in
521 this study. We thank Children's Healthcare of Atlanta, the Georgia Research Alliance,
522 and the Donaldson Trust for their support. The Emory Children's Center-Vaccine
523 Research Clinic also thanks Laila Hussaini, Ashley Tippett, Amy Muchinsky, and
524 Sydney Biccum for their assistance with this study. At the Hope clinic of Emory Vaccine
525 Center, we thank Rebecca Fineman, Dumingu Nipuni Gomes, Ellie Butler, Michelle
526 Wiles for their assistance with the study. At the Fred Hutchinson Cancer Research

527 Center, we thank Roland Strong for providing recombinant SARS-CoV-2 hexapro spike
528 (S6P) and Leo Stamatatos for providing RBD protein. We also thank Rebecca Putnam,
529 Todd Haight, Kim Louis, Ro Yoon, Carol Marty, Daryl Morris, Xiaoling Song, Mark
530 Majeres, Joe Abbott, Omolara Akingba, Josh Donahue, Tu Anh Nguyen, Katharine
531 Schwedhelm, Carly Sprague, and Terri Stewart for their vital assistance with this study.
532

533 **AUTHOR CONTRIBUTIONS**

534 M.J.M and R. Ahmed conceived the study. M.J.M., S.E., J.C., E.J.A., A.K.M, N.R. and
535 J.O.K. established the cohort and recruited the participants. S.L.L., M.P.L., C.W.D.,
536 M.P.G., S.G., K.A.S., G.M., C.N., V.V.E., L.L. and D.S.S. conducted serological assays
537 and related analyses. H.A., V.I.Z., B.P. and Z.M. conducted formal statistical analyses
538 and modeling. K.W.C., R.W. and L.E.N. planned, performed and analyzed antigen-
539 specific B cell flow cytometry. S.C.D., K.W.C. and S.F. conceived, supervised,
540 performed, and analyzed T cell experiments. V.E.E, K.F., and L.L. performed FRNT
541 assays. K.W.C., S.L.L. and Z.M. drafted the original manuscript; M.J.M., M.S.S. and
542 R.Ahmed edited the manuscript. All authors read and approved the manuscript. M.J.M.,
543 R.A, J.W. and M.S.S. secured funds and supervised the project.
544

545 **DECLARATION OF INTERESTS**

546 The authors declare no competing interests.
547

548 **FIGURE LEGENDS**

549 **Figure 1. Longitudinal SARS-CoV-2 spike binding antibody responses.**

550 IgG (A-C), IgA (D-F), and IgM (G-I) antibodies reactive to SARS-CoV-2 spike (A, D, G),
551 spike receptor binding domain (RBD; B, E, H), and the spike N terminal domain (NTD;
552 C, F, I) were measured by an electrochemiluminescent multiplex immunoassay and
553 reported as arbitrary units per ml (AU/ml) as normalized by a standard curve.
554 Longitudinal antibody titers of COVID-19 patients (in blue, n=222 COVID-19+ for IgG;
555 n=190 COVID-19+ for IgA and for IgM) are plotted over days since symptom onset,
556 whereas longitudinal pre-pandemic donor samples (in red, n=51 for IgG, IgA and IgM)
557 were collected in the course of a non-SARS-CoV-2 vaccine study before 2019 and
558 plotted over days since immunization. IgG decay curves and half-lives estimated by an
559 exponential decay model are shown in black, and the decay curves and half-lives at day
560 120 post symptom onset estimated by a power law model are shown in green.

561

562 **Figure 2. Longitudinal binding antibody responses to other coronavirus spike**
563 **proteins.**

564 IgG (A-E), IgA (F-J), and IgM (K-O) antibody responses in sera collected from COVID-
565 19+ patients (in blue, n=222 for IgG; n=190 for IgA and IgM) and pre-pandemic donors
566 (in red, n=51 for IgG, IgA and IgM) that were reactive to 229E spike (A, F, K), NL63
567 spike (B, G, L), HKU1 spike (C, H, M), OC43 spike (D, I, N), and the SARS-CoV-1 spike
568 protein (E, J, O). Antibody responses were measured by an electrochemiluminescent
569 multiplex immunoassay and reported as arbitrary units per ml (AU/ml) as normalized by
570 a standard curve. IgG decay curves and half-lives estimated by an exponential decay

571 model are shown in black. There was no significant decline in IgG reactive to endemic
572 alpha and betacoronaviruses in longitudinal samples collected in healthy donors before
573 the pandemic (red, A-D).
574
575 **Figure 3. Neutralizing antibody responses to SARS-CoV-2**
576 (A) *In vitro* serum neutralization antibody titers to SAR-CoV-2 were measured by focus-
577 reduction neutralization assay in 183 COVID-19 patients. The limit of detection is
578 indicated with a dashed line at FRNT-mNG_{50} = 20. The half-life estimated by the
579 exponential decay model (black) is 150 days, whereas the half-life estimated at day 120
580 using the power law model (green) is 254 days. IgG antibody titers reactive to SARS-
581 CoV-2 spike (B) and RBD (C) of the matched 183 COVID-19 for whom neutralization
582 titers were assessed. The geometric mean titer plus 3 standard deviations of pre-
583 pandemic samples is indicated by a dashed line (B and C). SARS-CoV-2 spike (D) and
584 RBD (E) reactive IgG levels correlated with neutralization titers at the matched time
585 point (repeated measures correlation, $p<0.0001$). The limit of detection is indicated with
586 a dashed line at FRNT-mNG_{50} = 20.
587
588 **Figure 4. SARS-CoV-2 spike and RBD specific memory B cells.**
589 (A) Representative memory B cell gating strategy is shown for identification of SARS-
590 CoV-2 spike and RBD-specific IgD- IgG+, IgD- IgM+ and IgD- IgA+ memory B cells in
591 PBMCs from a SARS-CoV-2 convalescent participant. The frequency of spike+ (B)
592 IgG+ and (C) IgM+ memory B cells out of memory B cells (IgD- CD19+ CD20+) is

593 displayed over time from initial symptom onset among SARS-CoV-2 infected subjects
594 (n=105 subjects). The dashed line indicates the limit of detection. The bold line
595 represents the median fitted curve from a linear mixed effects model of post-day 30
596 responses. (D) The median percent of spike+ memory B cells expressing IgG, IgM or
597 IgA isotypes was assessed at monthly intervals post-symptom onset. (E) The frequency
598 of RBD+ IgG+ of memory B cells over time (n=141). (F) The proportion of S+ IgG+
599 memory B cells that are specific for the receptor binding domain are depicted over time.
600
601 **Figure 5. CD4+ T cell responses to SARS-CoV-2 antigens.**
602 (A) The sum of background-subtracted CD4+ T cells expressing *ex vivo* IFN-γ, IL-2
603 and/or CD40L to peptide pools spanning SARS-CoV-2 structural proteins: S1, S2,
604 envelope (E), membrane (M), nucleocapsid (N), and the following ORFs: 3a, 3b, 6, 7a,
605 7b, and 8 (n=114) for each individual/timepoint. Each sample that is 'positive' (by
606 MIMOSA) for at least one SARS-CoV-2 antigen is indicated by a solid circle, whereas
607 samples that are 'negative' for all of the SARS-CoV-2 antigens at that timepoint are
608 indicated by open triangles. The bold line represents the median fitted curve from a
609 nonlinear mixed effects model of post-day 30 responses among those with a positive
610 response at >= 1 time point; $t_{1/2}$ is the median half-life estimated from the median slope,
611 with 95%CI [104, 411]. (B) The proportion of SARS-CoV-2-specific CD4+ T cells
612 expressing a specific memory phenotype over time: central memory (CCR7+ CD45RA-
613), effector memory (CCR7- CD45RA-) or T_{EMRA} (CCR7- CD45RA+); restricted to
614 'positive' responders. Polyfunctionality of SARS-CoV-2-specific CD4+ T cells are shown

615 at (C) 21-60 days since symptom onset (median, 30 days) and (D) >180 days median
616 post symptom onset (median, 203 days). Percentages of cytokine-expressing CD4+ T
617 cells are background subtracted and only subsets with detectable T cells are displayed.
618 Data shown were restricted to 'positive' responders and a single data point per
619 individual per time frame. All subsets were also evaluated for expression of IL-4, IL-5,
620 IL-13, IL-17 and perforin, and were found to be negative. (E) Bar graphs indicate the
621 proportion of COVID-19 convalescent patients who had a positive CD4+ T cell response
622 to the individual SARS-CoV-2. peptide pool *ex vivo* stimulations. Some antigens were
623 combined for stimulation as indicated. (F) For each subject with positive SARS-CoV-2-
624 specific CD4+ T cells, the proportion of the total SARS-CoV-2 responding CD4+ T cells
625 that are specific for each stimulation.
626
627 **Figure 6. CD8+ T cell responses to SARS-COV-2 antigens.**
628 (A) The sum of background-subtracted CD8+ T cells expressing IFN-γ (with or without
629 other cytokines), in response to peptide pools covering SARS-CoV-2 structural proteins:
630 S1, S2, envelope (E), membrane (M), nucleocapsid (N), and the following ORFs: 3a, 3b,
631 6, 7a, 7b, and 8 (n=114) for each individual/timepoint. Each sample that is 'positive'
632 (MIMOSA) for at least 1 SARS-CoV-2 antigen is indicated by a solid circle, whereas
633 samples that are 'negative' for all of the SARS-CoV-2 antigens at that timepoint are
634 indicated by open triangles. The bold black line represents the median fitted curve from
635 a nonlinear mixed effects model of post-day 30 responses among those with a positive
636 response to the antigen(s) under consideration at ≥ 1 time point; $t_{1/2}$ shown is the

637 median half-life estimated from the median slope, with 95%CI [92, 417]. (B) The
638 proportion of SARS-CoV-2-specific CD8+ T cells by memory phenotype over time:
639 effector memory (EM; CCR7- CD45RA-), T_{EMRA} (CCR7- CD45RA+) and central memory
640 (CM; CCR7+ CD45RA-). Analyses were restricted to 'positive' responders.
641 Polyfunctionality of SARS-CoV-2-specific CD8 T cells at (C) 21-60 days post symptom
642 onset (median, 30 days) and (D) >180 days median post symptom onset (median, 203
643 days). Percentages of cytokine expressing CD8+ T cells are background subtracted and
644 only subsets with detectable T cells are displayed. Data shown were restricted to
645 positive responders and a single data point per individual per time frame. All CD8+ T
646 cell subsets were also evaluated for expression of IL-4, IL-5, IL-13, and IL-17 and were
647 found to be negative. (E) The bar graphs indicate the proportion of COVID-19
648 convalescent patients who had a 'positive' CD8+ T cell response to the individual
649 SARS-CoV-2 stimulations. (F) The fraction of the total SARS-CoV-2 responding CD8+ T
650 cells per subject that are specific for each peptide pool.
651
652 **Figure 7. Correlations between SARS-CoV-2-specific immune responses and**
653 **assessment of covariates.**
654 (A) The forest plot depicts the estimated fold-change in the level of each immune
655 response per decade of age, with 95% Wald-based CIs and p-values. (B) The forest
656 plot shows the estimated fold-change in the level of each immune response for severe
657 (WHO score > 4) vs. non-severe (WHO score ≤ 4) disease, with 95% Wald-based CIs
658 and p-values. S1 CD8+ T cell responses compared moderate-severe (WHO score > 2)

659 to mild (WHO score ≤ 2) disease as there were no participants with severe disease with
660 at least one positive S1 CD8+ T cell response post-day 30. Estimates in (A) and (B) are
661 from mixed effects models of post-day 30 (B and T cell responses) or post-day 42
662 (antibody responses) among responders that account for fixed effects of age and
663 disease severity on the level of immune response. Univariate assessment of disease
664 severity on the magnitude of (C) spike IgG antibodies and (D) SARS-CoV-2 neutralizing
665 antibodies at day 120 is shown for mild (WHO score: 0-2), moderate (WHO score: 3-4),
666 and severe disease (WHO score: 5+); p-values from one-way ANOVA. (E) The heatmap
667 shows Spearman correlations between critical SARS-CoV-2 memory immune
668 responses (day 30 B and T cell responses and day 180 antibody responses) with
669 significance levels: *p<0.05, **p<0.01, ***p<0.001. The tile size and color intensity
670 correspond to the absolute value of the Spearman rank correlation coefficient, with red
671 or blue indicating a positive or negative correlation, respectively. Day 30, 42 and 180
672 immune responses were estimated from mixed effects models of the longitudinal SARS-
673 CoV-2 binding antibodies, SARS-CoV-2 neutralizing antibodies, CD4+ and CD8+ T
674 cell responses, and B cell responses.
675

676 **METHODS DESRIPTIONS**

677 **Study Populations**

678 Two longitudinal COVID-19 cohort studies at Fred Hutchinson Cancer Research
679 Center (Seattle, Washington) and Emory University (Atlanta, Georgia) began after
680 receiving institutional review board approvals (IRB 10440, IRB 00001080 and

681 IRB00022371). Adults ≥18 years were enrolled who met eligibility criteria for SARS-
682 CoV-2 infection and provided informed consent. Study participants provided medical
683 history of co-morbidities, presentation of SARS-CoV-2 infection onset and disease
684 course, and peripheral blood at initial and follow up visits for analysis of serum antibody
685 and cellular immune responses. Additional longitudinal archived sera and PBMC from
686 pre-pandemic study populations from Emory and Seattle served as controls for the
687 immune assays.

688 The Atlanta study population included adult volunteers over the age of 18 who were
689 diagnosed with COVID-19 by a commercially available SARS CoV-2 PCR assay, rapid
690 antigen test, or clinical syndrome only (later confirmed with serology) due to limited
691 SARS-CoV-2 testing during the early period of the pandemic. Ambulatory participants
692 were recruited through local advertisements, internet-based avenues (such as social
693 media, list serves), COVID-19 testing sites, and primary care clinics. Hospitalized
694 patients were identified through SARS-CoV-2 testing. Informed consent was obtained
695 from all participants prior to conduct of study procedures. Initial acute peripheral blood
696 samples were collected from hospitalized patients at the time of enrollment.
697 Convalescent samples from hospitalized patients were collected when the patients were
698 able to return for a visit to the clinical research site at the next study visit. Serial
699 peripheral blood samples were collected starting at about 30 days after the onset of
700 COVID-19 symptoms and/or after PCR positivity for SARS-CoV-2. Thereafter, samples
701 were collected at 3, 6, and 9 months. The study is ongoing with expected completion of
702 sample collection from participants in February 2023. Participants were excluded if they

703 were immunocompromised, HIV positive, had active hepatitis B or C virus infection,
704 used immunosuppressive drugs for 2 weeks or more in the preceding 3 months,
705 received blood products or immune globulin 42 days prior to enrollment, received
706 convalescent COVID-19 plasma, or were pregnant or breast feeding. We report on 110
707 participants to date, of which 73% were diagnosed by SARS-CoV-2 PCR, the remaining
708 were diagnosed by rapid antigen test or serology. Demographic features of the
709 participants are as follows: median age was 48; 45% were male; the majority (80%)
710 were white, 11% Black/African American, 6% Asian, and 8% were Hispanic/Latinx
711 ethnicity. The most frequent co-morbid conditions were hypertension, obesity, heart
712 disease and diabetes mellitus. The most frequent COVID-19 symptoms were
713 myalgia/fatigue, fever, cough, headache, loss of smell and taste (Table S1).
714 Hospitalized patients were older, with a median age of 56; a higher percentage were
715 Black/African American (27%); and 100% had fever.
716 Longitudinal pre-pandemic sera samples from Emory were collected from
717 individuals participating in a yellow fever vaccine study from 2014-2016 or an influenza
718 vaccine study from 2015-2018 (Akondy et al., 2017; Ellebedy et al., 2016). Data were
719 included for analysis of binding antibody responses and are presented as days post-
720 irrelevant (yellow fever) vaccination.
721 The Seattle COVID-19 Cohort study participants were recruited from the Seattle
722 metropolitan area by social media advertisements, partnership with the local emergency
723 medical service and by word of mouth. Study participants were screened and enrolled
724 by the Seattle Vaccine Trials Unit staff. Eligibility criteria included adults at risk for

725 SARS-CoV-2 infection or those diagnosed with COVID-19 by a commercially available
726 SARS-CoV-2 PCR assay or blood antibody test and willing to have at least four blood
727 draws collected over one year. Exclusion criteria included pregnancy and inability to
728 donate blood.

729 Informed electronic consent was obtained from all Seattle participants during a
730 screening phone call with study clinical staff. Interested participants were screened,
731 consented and medical history and COVID-19 illness onset date and symptoms
732 collected. Participants undiagnosed with COVID-19 had a nasopharyngeal (NP) swab
733 collected and tested for SARS-CoV-2 via an FDA-approved PCR test and blood was
734 collected for SARS-CoV-2 antibody (Abbott) and study assays. Those with either a
735 positive PCR or antibody test were asked to return for future blood draws. Those who
736 tested negative were asked to return as controls for the positive cohort and in case they
737 tested positive in the future. Participants with a positive test prior to study enrollment or
738 those diagnosed in study were asked to provide blood donation at approximately 7
739 days, 2 weeks, 1, 2, 3, 4, 6, 9- and 12-months post symptom onset. After completing
740 one year of study, participants will be given the option of continuing the longitudinal
741 study for up to two or more years. At each study visit, participant symptoms and medical
742 history is updated. Those with COVID-19 symptoms after enrollment in all groups are
743 offered a nasopharyngeal swab PCR SARS-CoV-2 test.

744 As of October 2020, 805 individuals have contacted the Seattle COVID-19 cohort
745 study and 425 have enrolled. This includes 281 negative and 144 SARS-CoV-2 positive
746 participants. Reasons for not enrolling include lack of interest, not meeting the eligibility

747 criteria, inability to travel to blood draw location and inability to collect study blood. No
748 participants have terminated from the study. Study enrollment and follow-up remains
749 ongoing. Samples from SARS-CoV-2 negative subjects were included in B and T cell
750 assays as 'contemporaneous' negative controls.

751 Peripheral blood mononuclear cells (PBMC) were obtained from HIV-1 seronegative
752 donors who were recruited at the Seattle Vaccine Trials Unit before 2019 as part of the
753 study "Establishing Immunologic Assays for Determining HIV-1 Prevention and Control".
754 All participants signed informed consent, and the Fred Hutchinson Cancer Research
755 Center IRB (Seattle, WA, USA) institutional human subjects review committee approved
756 the protocol prior to study initiation. Pre-pandemic samples from this cohort were used
757 as assay controls in B and T cell assays.

758

759 **PBMC processing**

760 PBMC for cellular assays were isolated by density centrifugation and cryopreserved
761 from ACD-anticoagulated whole blood within eight hours of venipuncture, as described
762 previously (Cross-Network PBMC SOP Working Group, 2018). Sera were also
763 processed and cryopreserved within 4 hours after collection.

764

765 **Antibody binding assay**

766 Antibody binding titers were measured using a multiplex plate coated with the SARS-
767 CoV-2 spike, SARS-CoV-2 spike receptor binding domain, SARS-CoV-2 spike N
768 terminal domain, SARS-CoV-2 nucleocapsid, SARS-CoV-1 spike, 229E spike, NL63

769 spike, HKU1 spike, and OC43 spike proteins (Mesoscale Discovery). Plates were
770 blocked with 150µl/well with 5% bovine serum albumin in phosphate buffered saline
771 (PBS) and shaken at 700 RPM at room temperature for at least 30 min. Plates were
772 washed 3 times with 150µl/well 0.05% Tween-20 in PBS. Serum and plasma samples
773 were added to the plate at dilutions between 1:500 and 1:50,000 and shaken at 700
774 RPM at room temperature for 2 hr. Following a wash, plates were incubated with
775 50ul/well of Sulfo-Tag anti-human IgG, IgA, or IgM detection antibody and shaken at
776 700RPM at room temperature for 1 hr. After a subsequent wash, 150µl/well of MSD
777 GOLD read buffer was added to the plate and plates were immediately read on the
778 MSD instrument to measure light intensity. Antibody levels are reported as arbitrary
779 units/ml (AU/ml) based on normalization to a standard curve.
780
781 **Viruses and cells**
782 VeroE6 cells were obtained from ATCC (clone E6, ATCC, #CRL-1586) and cultured in
783 complete DMEM medium consisting of 1× DMEM (VWR, #45000-304), 10% FBS,
784 25mM HEPES Buffer (Corning Cellgro), 2mM L-glutamine, 1mM sodium pyruvate, 1×
785 Non-essential Amino Acids, and 1× antibiotics. The infectious clone SARS-CoV-2
786 (icSARS-CoV-2-mNG), derived from the 2019-nCoV/USA_WA1/2020 strain, was
787 propagated in VeroE6 cells (ATCC) and sequenced (Xie et al., 2020).
788
789 **Focus reduction neutralization test**

790 Neutralization assays with SARS-CoV-2 virus were performed as previously described
791 (Suthar et al., 2020; Vanderheiden et al., 2020; Xie et al., 2020). Plasma/serum were
792 serially diluted (three-fold) in serum-free Dulbecco's modified Eagle's medium (DMEM)
793 in duplicate wells and incubated with 100–200 FFU infectious clone derived SARS-CoV-
794 2-mNG virus at 37°C for 1 hr (Xie et al., 2020). The antibody-virus mixture was added to
795 VeroE6 cell (C1008, ATCC, #CRL-1586) monolayers seeded in 96-well blackout plates
796 and incubated at 37°C for 1 hr. Post-incubation, the inoculum was removed and
797 replaced with pre-warmed complete DMEM containing 0.85% methylcellulose. Plates
798 were incubated at 37°C for 24 hr. After 24 hr, methylcellulose overlay was removed,
799 cells were washed twice with PBS and fixed with 2% paraformaldehyde in PBS for
800 30 min at room temperature. Following fixation, plates were washed twice with PBS and
801 foci were visualized on a fluorescence ELISPOT reader (CTL ImmunoSpot S6 Universal
802 Analyzer) and enumerated using Viridot (Katzelnick et al., 2018). The neutralization
803 titers were calculated as follows: 1 - (ratio of the mean number of foci in the presence of
804 sera and foci at the highest dilution of respective sera sample). Each specimen was
805 tested in two independent assays performed at different times. The FRNT-mNG$_{50}$ titers
806 were interpolated using a 4-parameter nonlinear regression in GraphPad Prism
807 8.4.3. Samples with an FRNT-mNG$_{50}$ value that was below the limit of detection were
808 plotted at 20.
809
810 **Spike and RBD memory B cell flow cytometry assays**

811 Fluorescent SARS-CoV-2-specific S6P (Hsieh et al., 2020) (provided by Roland Strong,
812 Fred Hutchinson Cancer Research Center, Seattle, WA) and RBD (provided by
813 Leonidas Stamatatos, Fred Hutchinson Cancer Research Center, Seattle, WA) probes
814 were made by combining biotinylated protein with fluorescently labeled streptavidin
815 (SA). The S6P probes were made at a ratio of 1:1 molar ratio of trimer to SA. Two S6P
816 probes, one labeled with AlexaFluor488 (Invitrogen), one labeled with AlexaFluor647
817 (Invitrogen), were used in this panel in order to increase specificity of the detection of
818 SARS-CoV-2-specific B cells. The RBD probe was prepared at a 4:1 molar ratio of RBD
819 monomers to SA, labeled with R-phycoerythrin (Invitrogen). Cryopreserved PBMCs
820 from SARS-CoV-2-convalescent participants and a pre-pandemic SARS-CoV-2-naïve
821 donor were thawed at 37°C and stained for SARS-CoV-2-specific memory B cells as
822 described previously (Seydoux et al., 2020) with a flow cytometry panel shown in
823 Reagents Table 1. Cells were stained first with the viability stain (Invitrogen) in PBS for
824 15 min at 4°C. Cells were then washed with 2% FBS/PBS and stained with a cocktail of
825 the three probes for 30 min at 4°C. The probe cocktail was washed off with 2%
826 FBS/PBS and the samples were stained with the remaining antibody panel and
827 incubated for 25 min at 4°C. The cells were washed two times and resuspended in 1%
828 paraformaldehyde/1× PBS for collection on a LSR II or FACSymphony flow cytometer
829 (BD Biosciences). Data was analyzed in Flow Jo version 9.9.4.
830
831 **Intracellular cytokine staining (ICS) assay**

832 Flow cytometry was used to examine SARS-CoV-2-specific CD4+ and CD8+ T-cell
833 responses using a validated ICS assay. The assay was similar to a published report
834 (Dintwe et al., 2019; Horton et al., 2007; Sadoff et al., 2021) and the details of the
835 staining panel are included in Reagents Table 2. Peptide pools covering the structural
836 proteins of SARS-CoV-2 were used for the six-hour stimulation. Peptides matching the
837 SARS-CoV-2 spike sequence (316 peptides, plus 4 peptides covering the G614 variant)
838 were synthesized as 15 amino acids long with 11 amino acids overlap and pooled in 2
839 pools (S1 and S2) for testing (BioSynthesis). All other peptides were 13 amino acids
840 overlapping by 11 amino acids and were synthesized by GenScript. The peptides
841 covering the envelope (E), membrane (M) and nucleocapsid (N) were initially combined
842 into one peptide pool, but the majority of the assays were performed using a separate
843 pool for N and one that combined only E and M. Several of the open reading frame
844 (ORF) peptides were combined into two pools: ORF 3a and 6, and ORF 7a, 7b and 8.
845 All peptide pools were used at a final concentration of 1 μg/ml for each peptide. As a
846 negative control, cells were not stimulated, only the peptide diluent (DMSO) was
847 included. As a positive control, cells were stimulated with a polyclonal stimulant,
848 staphylococcal enterotoxin B (SEB). Cells expressing IFN-γ and/or IL-2 and/or CD154
849 was the primary immunogenicity endpoint for CD4+ T cells and cells expressing IFN-γ
850 was the primary immunogenicity endpoint for CD8+ T cells. The overall response to
851 SARS-CoV-2 was defined as the sum of the background-subtracted responses to each
852 of the individual pools. A sample was considered positive for CD4+ or CD8+ T cell
853 responses to SARS-CoV-2 if any of the CD4+ or CD8+ T cell responses to the

854 individual peptide pool stimulations was positive. Positivity was determined using
855 MIMOSA (Finak et al., 2014). The total number of CD4+ T cells must have exceeded
856 10,000 and the total number of CD8+ T cells must have exceeded 5,000 for the assay
857 data to be included in the analysis.
858
859 **Statistical methods**
860 *Binding and neutralizing antibody responses*
861 Mixed effects exponential and power law models were used to analyze waning of
862 antibody (day 42 to day 263 post symptom onset). For binding antibody analyses,
863 antibody (Ab) was natural log transformed, yielding linear equations of the form
864 ln(Ab)=a+b*(day-42) and ln(Ab)=a+b*ln(day/42) for the exponential and power law
865 models, respectively, and fit using the lmer function (lme4 package) in R. Models
866 included population level fixed effects and individual level random effects for intercept
867 and slope and covariance between the random effects. Simplified models – with random
868 effects only for intercept – were also fit. Neutralization antibody data were analyzed in
869 Monolix (Lixoft). For analysis in Monolix, the exponential and power law models were
870 formulated as ordinary differential equations, dAb/dt=k*Ab and dAb/dt=k*Ab/t,
871 respectively, with antibody at day 42 lognormally distributed and lognormal multiplicative
872 error. Neutralization titers < 20 were treated as left censored. For comparison of
873 models, difference in Akaike information criterion (ΔAIC) > 4 was considered statistically
874 significant. Models (in R and Monolix) were fit using maximum likelihood. To account for
875 repeated measures, correlations between antibody binding levels and neutralization

titers were calculated using a repeated measures correlation (rmcorr package) in R (Bakdash and Marusich, 2017).

B cell responses

We considered linear mixed effects models for B cell response, $\mathcal{Y}_{ij}$, as a function of t_{ij}, the jth time since symptom onset for the ith individual, with random effects for intercept and slope and t_{ij} > 30 days for all i, j:

$$\log_e \mathcal{Y}_{ij} = \beta_{0i} + \beta_{1i} t_{ij} + \epsilon_{ij}$$

where $\beta_{0i} = \beta_0 + b_i$ and $\beta_{1i} = \beta_1 + c_i$ with (b_i, c_i) iid ~ $N_2(\mathbf{0}, \mathbf{\Sigma})$, with

$$\mathbf{\Sigma} = \begin{bmatrix} \sigma_b^2 & Cov(b,c) \\ Cov(b,c) & \sigma_c^2 \end{bmatrix}$$

and σ_b^2 and σ_c^2 are the between-person variation in the intercept and slope of log B cell responses respectively, *Cov(b, c)* is the covariance between the intercept and slope, and ϵ_{ij} iid ~ $N(0, \sigma^2)$. The random effects, b_i and c_i, are each assumed to be independent for different individuals and the within-individual errors ϵ_{ij} are assumed to be independent for different *i, j* and to be independent of the random effects. The function lme from the R package nlme was used to fit the model.

T cell responses

Longitudinal analyses of CD4+ and CD8+ T cell responses were performed for individuals with a positive response for at least one time point 30 days after symptom

onset. The MIMOSA (Mixture Models for Single-Cell Assays) (Finak et al., 2014) model incorporated cell count and cell proportion information to define a positive CD4+/CD8+ T cell response by ICS by comparing peptide pools stimulated cells and unstimulated negative controls. This method assumed a common distribution for cytokine positive CD4+/CD8+ T cells in stimulated and unstimulated samples in non-responders, resulting in paired differences that were zero on average. In contrast, for responders, the distribution of the proportion of cytokine positive cells for stimulated samples was assumed to be greater than for unstimulated samples, resulting in paired differences that were greater than zero on average. The MIMOSA method modeled this structure through a Bayesian hierarchical mixture model framework. One component (or distribution) of the model represented the responders, and the other component modeled the non-responders. The parameters defining these distributions, as well as the probabilities that each ICS response was either a responder or non-responder, were estimated from the observed data. This sharing of information across SARS-CoV-2 responders and non-responders increased the sensitivity and specificity to make positivity calls (Newton et al., 2004). Responses with probability of response > 0.999 were considered positive responders.

We considered nonlinear mixed effects models for T cell response, $\mathcal{Y}_{ij}$, as a function of t_{ij}, the jth time since symptom onset for the ith individual, with random effects for intercept and slope and t_{ij} > 30 days for all i, j:

$$\log_e \mathcal{Y}_{ij} = \beta_{0i} - \exp(\beta_{1i})\, t_{ij} + \epsilon_{ij}$$

where $\beta_{0i} = \beta_0 + b_i$ and $exp(\beta_{1i}) = exp(\beta_1 + c_i)$ with (b_i, c_i) iid ~ $N_2(\mathbf{0}, \mathbf{\Sigma})$, with

$$\mathbf{\Sigma} = \begin{bmatrix} \sigma_b^2 & 0 \\ 0 & \sigma_c^2 \end{bmatrix}$$

and σ_b^2 and σ_c^2 are the between-person variation in the intercept and slope of log T cell responses respectively, and ϵ_{ij} iid ~ $logNormal(0, \sigma^2)$. The random effects, b_i and c_i, are each assumed to be independent for different individuals and the within-individual errors ϵ_{ij} are assumed to be independent for different *i, j* and to be independent of the random effects. The function nlme from the R package nlme was used to fit the models. Individual-level estimates at days 30 (T and B cell responses), day 42 (antibody responses) and day 180 (all responses) were obtained from the mixed effects models described above. Spearman rank correlations, Wald-based two-sided 95% confidence intervals and p-values were reported.

Generalized estimating equations (GEE), with an independence working covariance matrix, were used to confirm the results of the covariate assessments for B and T cell responses from the mixed effects models. Two-tailed P-values based on the robust standard error estimates for the covariate coefficients were consistent with the corresponding two-tailed P-values for the covariate associations from the mixed effects models.

936 **Reagents Table 1. Reagents used in the B cell staining panel.**

Antibody	Manufacturer	Clone
CD3 BV510	BD Biosciences	HIT3a
CD14 BV510	BD Biosciences	MφP9
CD56 BV510	BD Biosciences	NCAM16.2
CD19 BUV395	BD Biosciences	SJ25-C1
CD20 BUV737	BD Biosciences	2H7
CD21 PE-Cy7	BD Biosciences	B-ly4
CD27 BV605	BioLegend	O323
CD38 BB700	BD Biosciences	HIT2
IgA VioBlue	Miltenyi Biotec	IS11-8E10
IgD BV650	BD Biosciences	IA6-2
IgG BV786	BD Biosciences	G18-145
IgM PE/Dazzle 594	BioLegend	MHM-88
R-Phycoerythrin Streptavidin	Invitrogen	N/A
AlexaFluor 488 Streptavidin	Invitrogen	N/A
AlexaFluor 647 Streptavidin	Invitrogen	N/A
LIVE/DEAD Fixable Aqua Stain	Invitrogen	N/A

937 *APC, allophycocyanin; BB, brilliant blue; BUV, brilliant ultraviolet; BV, brilliant violet; Cy, cyanine;*
938 *FITC, fluorescein isothiocyanate; PE R-phycoerythrin; UViD, Live/Dead fiaxable ultraviolet dead cell*
939 *stain*
940

941 **Reagents Table 2. T cell intracellular cytokine staining flow cytometry panel.**

Detector	Fluorochrome	Specificity	Clone	Purpose
B515	FITC	Perforin	B-D48	Function
B610	BB630	IL-5	TRFK5	Function
B610	BB630	IL-13	JES10-5A2	Function
B660	BB660	Ki67	B56	Activation
B710	BB700	IL-4	MP4-25D2	Function
G575	PE	CRTh2	BM16	T helper class
G610	PE-Dazzle594	CD32	FUN-2	Fcg receptor
G660	Pe-Cy5	CXCR3 (CD183)	1C6/CXCR3	T helper class
G710	PE-Cy5.5	FOXP3	PCH101	Treg
G780	PE-Cy7	IL-17a	BL168	Function
R660	APC	IL-2	MQ1-17H12	Function
R710	Alexa 700	Granzyme B	GB11	Function
R780	APC-Fire750	CD3	UCHT1	T cell lineage
U395	BUV395	TNF	MAb11	Function
U450	UViD	Viability	N/A	Viability
U500	BUV496	CD45RA	HI100	Differentiation
U570	BUV563	CD19	SJ25C1	B cells
U660	BUV661	CD14	MFP9	Monocytes
U730	BUV737	CD154	TRAP1	Function
U780	BUV805	CD8	SK1	T cell lineage
V450	V450	IFN-γ	B27	Function
V510	BV480	CD4	SK3	Function
V570	BV570	CD16	3G8	NK, NKT
V610	BV605	CCR7	G034H7	Differentiation
V655	BV650	CD25	M-A251	Treg, activation
V710	BV711	CD64	10.1	Fcg receptor
V750	BV750	CD56	5.1H11	NK, NKT
V780	BV786	CCR6 (CD196)	11A9	T helper class

942

943 **References**

944 Akondy, R.S., Fitch, M., Edupuganti, S., Yang, S., Kissick, H.T., Li, K.W., Youngblood,
945 B.A., Abdelsamed, H.A., McGuire, D.J., Cohen, K.W.*, et al.* (2017). Origin and
946 differentiation of human memory CD8 T cells after vaccination. Nature *552*, 362-367.

947 Amanna, I.J., Carlson, N.E., and Slifka, M.K. (2007). Duration of humoral immunity to
948 common viral and vaccine antigens. N Engl J Med *357*, 1903-1915.

949 Anderson, E.J., Rouphael, N.G., Widge, A.T., Jackson, L.A., Roberts, P.C., Makhene,
950 M., Chappell, J.D., Denison, M.R., Stevens, L.J., Pruijssers, A.J.*, et al.* (2020). Safety
951 and Immunogenicity of SARS-CoV-2 mRNA-1273 Vaccine in Older Adults. *383*, 2427-
952 2438.

953 Bakdash, J.Z., and Marusich, L.R. (2017). Repeated Measures Correlation. Front
954 Psychol *8*, 456.

955 Callow, K.A., Parry, H.F., Sergeant, M., and Tyrrell, D.A. (1990). The time course of the
956 immune response to experimental coronavirus infection of man. Epidemiol Infect *105*,
957 435-446.

958 Cross-Network PBMC SOP Working Group (2018). Cross-Network PBMC Processing
959 SOP v6.0. HIV/AIDS Network Coordination (HANC)
960 *https://www.hanc.info/labs/Documents/PBMC%20Documents/HANC-LAB-*
961 *P0001_v6.0_2018-04-26_PBMC_SOP.pdf*.

962 Dan, J.M., Mateus, J., Kato, Y., Hastie, K.M., Yu, E.D., Faliti, C.E., Grifoni, A., Ramirez,
963 S.I., Haupt, S., Frazier, A.*, et al.* (2021). Immunological memory to SARS-CoV-2
964 assessed for up to 8 months after infection. Science *371*.

965 Davis, C.W., Jackson, K.J.L., McCausland, M.M., Darce, J., Chang, C., Linderman,
966 S.L., Chennareddy, C., Gerkin, R., Brown, S.J., Wrammert, J.*, et al.* (2020). Influenza
967 vaccine-induced human bone marrow plasma cells decline within a year after
968 vaccination. Science *370*, 237-241.

969 Dintwe, O., Rohith, S., Schwedhelm, K.V., McElrath, M.J., Andersen-Nissen, E., and De
970 Rosa, S.C. (2019). OMIP-056: Evaluation of Human Conventional T Cells, Donor-
971 Unrestricted T Cells, and NK Cells Including Memory Phenotype by Intracellular
972 Cytokine Staining. Cytometry A *95*, 722-725.

973 Doria-Rose, N., Suthar, M.S., Makowski, M., O'Connell, S., McDermott, A.B., Flach, B.,
974 Ledgerwood, J.E., Mascola, J.R., Graham, B.S., Lin, B.C.*, et al.* (2021). Antibody
975 Persistence through 6 Months after the Second Dose of mRNA-1273 Vaccine for Covid-
976 19. N Engl J Med.

977 Edara, V.V., Norwood, C., Floyd, K., Lai, L., Davis-Gardner, M.E., Hudson, W.H.,
978 Mantus, G., Nyhoff, L.E., Adelman, M.W., Fineman, R.*, et al.* (2021). Infection- and
979 vaccine-induced antibody binding and neutralization of the B.1.351 SARS-CoV-2
980 variant. Cell Host Microbe *29*, 516-521 e513.

981 Edridge, A.W.D., Kaczorowska, J., Hoste, A.C.R., Bakker, M., Klein, M., Loens, K.,
982 Jebbink, M.F., Matser, A., Kinsella, C.M., Rueda, P.*, et al.* (2020). Seasonal coronavirus
983 protective immunity is short-lasting. Nat Med *26*, 1691-1693.

984 Ellebedy, A.H., Jackson, K.J., Kissick, H.T., Nakaya, H.I., Davis, C.W., Roskin, K.M.,
985 McElroy, A.K., Oshansky, C.M., Elbein, R., Thomas, S.*, et al.* (2016). Defining antigen-
986 specific plasmablast and memory B cell subsets in human blood after viral infection or
987 vaccination. Nat Immunol *17*, 1226-1234.

988 Finak, G., McDavid, A., Chattopadhyay, P., Dominguez, M., De Rosa, S., Roederer, M.,
989 and Gottardo, R. (2014). Mixture models for single-cell assays with applications to
990 vaccine studies. Biostatistics *15*, 87-101.

991 Gaebler, C., Wang, Z., Lorenzi, J.C.C., Muecksch, F., Finkin, S., Tokuyama, M., Cho,
992 A., Jankovic, M., Schaefer-Babajew, D., Oliveira, T.Y.*, et al.* (2021). Evolution of
993 antibody immunity to SARS-CoV-2. Nature *591*, 639-644.

994 Hammarlund, E., Lewis, M.W., Hansen, S.G., Strelow, L.I., Nelson, J.A., Sexton, G.J.,
995 Hanifin, J.M., and Slifka, M.K. (2003). Duration of antiviral immunity after smallpox
996 vaccination. Nat Med *9*, 1131-1137.

997 Horton, H., Thomas, E.P., Stucky, J.A., Frank, I., Moodie, Z., Huang, Y., Chiu, Y.L.,
998 McElrath, M.J., and De Rosa, S.C. (2007). Optimization and validation of an 8-color
999 intracellular cytokine staining (ICS) assay to quantify antigen-specific T cells induced by
1000 vaccination. J Immunol Methods *323*, 39-54.

1001 Hsieh, C.L., Goldsmith, J.A., Schaub, J.M., DiVenere, A.M., Kuo, H.C., Javanmardi, K.,
1002 Le, K.C., Wrapp, D., Lee, A.G., Liu, Y.*, et al.* (2020). Structure-based design of
1003 prefusion-stabilized SARS-CoV-2 spikes. Science *369*, 1501-1505.

1004 Ju, B., Zhang, Q., Ge, J., Wang, R., Sun, J., Ge, X., Yu, J., Shan, S., Zhou, B., Song,
1005 S.*, et al.* (2020). Human neutralizing antibodies elicited by SARS-CoV-2 infection.
1006 Nature *584*, 115-119.

1007 Katzelnick, L.C., Coello Escoto, A., McElvany, B.D., Chavez, C., Salje, H., Luo, W.,
1008 Rodriguez-Barraquer, I., Jarman, R., Durbin, A.P., Diehl, S.A.*, et al.* (2018). Viridot: An
1009 automated virus plaque (immunofocus) counter for the measurement of serological
1010 neutralizing responses with application to dengue virus. PLoS Negl Trop Dis *12*,
1011 e0006862.

1012 Lavine, J.S., Bjornstad, O.N., and Antia, R. (2021). Immunological characteristics
1013 govern the transition of COVID-19 to endemicity. Science *371*, 741-745.

1014 Manz, R.A., Thiel, A., and Radbruch, A. (1997). Lifetime of plasma cells in the bone
1015 marrow. Nature *388*, 133-134.

1016 Mascola, J.R., Graham, B.S., and Fauci, A.S. (2021). SARS-CoV-2 Viral Variants-
1017 Tackling a Moving Target. JAMA *325*, 1261-1262.

1018 Newton, M.A., Noueiry, A., Sarkar, D., and Ahlquist, P. (2004). Detecting differential
1019 gene expression with a semiparametric hierarchical mixture method. Biostatistics *5*,
1020 155-176.

1021 Rodda, L.B., Netland, J., Shehata, L., Pruner, K.B., Morawski, P.A., Thouvenel, C.D.,
1022 Takehara, K.K., Eggenberger, J., Hemann, E.A., Waterman, H.R.*, et al.* (2021).
1023 Functional SARS-CoV-2-Specific Immune Memory Persists after Mild COVID-19. Cell
1024 *184*, 169-183 e117.

1025 Sadoff, J., Le Gars, M., Shukarev, G., Heerwegh, D., Truyers, C., de Groot, A.M.,
1026 Stoop, J., Tete, S., Van Damme, W., Leroux-Roels, I.*, et al.* (2021). Interim Results of a
1027 Phase 1-2a Trial of Ad26.COV2.S Covid-19 Vaccine. N Engl J Med.

1028 Sette, A., and Crotty, S. (2021). Adaptive immunity to SARS-CoV-2 and COVID-19. Cell
1029 *184*, 861-880.

1030 Seydoux, E., Homad, L.J., MacCamy, A.J., Parks, K.R., Hurlburt, N.K., Jennewein,
1031 M.F., Akins, N.R., Stuart, A.B., Wan, Y.H., Feng, J.*, et al.* (2020). Analysis of a SARS-
1032 CoV-2-Infected Individual Reveals Development of Potent Neutralizing Antibodies with
1033 Limited Somatic Mutation. Immunity *53*, 98-105 e105.

1034 Slifka, M.K., Antia, R., Whitmire, J.K., and Ahmed, R. (1998). Humoral immunity due to
1035 long-lived plasma cells. Immunity *8*, 363-372.

1036 Stamatatos, L., Czartoski, J., Wan, Y.H., Homad, L.J., Rubin, V., Glantz, H., Neradilek,
1037 M., Seydoux, E., Jennewein, M.F., MacCamy, A.J.*, et al.* (2021). mRNA vaccination
1038 boosts cross-variant neutralizing antibodies elicited by SARS-CoV-2 infection. Science.

1039 Stephens, D.S., and McElrath, M.J. (2020). COVID-19 and the Path to Immunity. JAMA
1040 *324*, 1279-1281.

1041 Suthar, M.S., Zimmerman, M.G., Kauffman, R.C., Mantus, G., Linderman, S.L., Hudson,
1042 W.H., Vanderheiden, A., Nyhoff, L., Davis, C.W., Adekunle, O.*, et al.* (2020). Rapid
1043 Generation of Neutralizing Antibody Responses in COVID-19 Patients. Cell Rep Med *1*,
1044 100040.

1045 Vanderheiden, A., Edara, V.V., Floyd, K., Kauffman, R.C., Mantus, G., Anderson, E.,
1046 Rouphael, N., Edupuganti, S., Shi, P.Y., Menachery, V.D.*, et al.* (2020). Development of
1047 a Rapid Focus Reduction Neutralization Test Assay for Measuring SARS-CoV-2
1048 Neutralizing Antibodies. Curr Protoc Immunol *131*, e116.

1049 Veit, O., Domingo, C., Niedrig, M., Staehelin, C., Sonderegger, B., Hequet, D., Stoeckle,
1050 M., Calmy, A., Schiffer, V., Bernasconi, E.*, et al.* (2018). Long-term Immune Response
1051 to Yellow Fever Vaccination in Human Immunodeficiency Virus (HIV)-Infected
1052 Individuals Depends on HIV RNA Suppression Status: Implications for Vaccination
1053 Schedule. Clinical infectious diseases : an official publication of the Infectious Diseases
1054 Society of America *66*, 1099-1108.

1055 Walls, A.C., Park, Y.J., Tortorici, M.A., Wall, A., McGuire, A.T., and Veesler, D. (2020).
1056 Structure, Function, and Antigenicity of the SARS-CoV-2 Spike Glycoprotein. Cell *181*,
1057 281-292 e286.

1058 Xie, X., Muruato, A., Lokugamage, K.G., Narayanan, K., Zhang, X., Zou, J., Liu, J.,
1059 Schindewolf, C., Bopp, N.E., Aguilar, P.V.*, et al.* (2020). An Infectious cDNA Clone of
1060 SARS-CoV-2. Cell Host Microbe *27*, 841-848 e843.

1061 Zarnitsyna, V.I., Akondy, R.S., Ahmed, H., McGuire, D.J., Zarnitsyn, V.G., Moore, M.,
1062 Johnson, P.L.F., Ahmed, R., Li, K., Hellerstein, M.*, et al.* (2021). Dynamics and turnover
1063 of memory CD8 T cell responses following yellow fever vaccination. bioRxiv,
1064 2021.2001.2023.427919.

1065 Zost, S.J., Gilchuk, P., Case, J.B., Binshtein, E., Chen, R.E., Nkolola, J.P., Schafer, A.,
1066 Reidy, J.X., Trivette, A., Nargi, R.S.*, et al.* (2020). Potently neutralizing and protective
1067 human antibodies against SARS-CoV-2. Nature *584*, 443-449.

1068

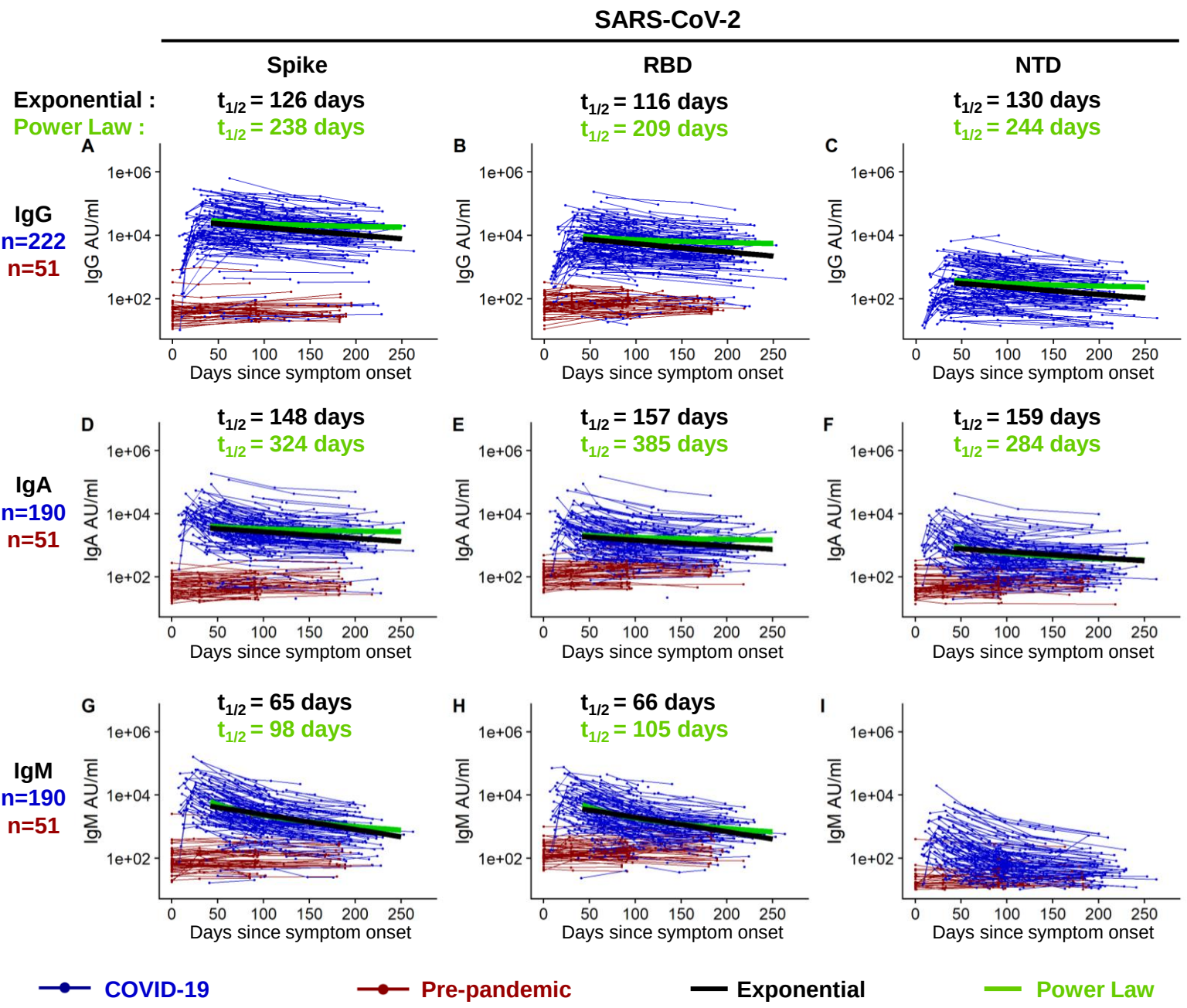
SARS-CoV-2
Spike
RBD
NTD
Exponential :
Power Law :
A
$t_{1/2}$ = 126 days
$t_{1/2}$ = 238 days
B
$t_{1/2}$ = 116 days
$t_{1/2}$ = 209 days
C
$t_{1/2}$ = 130 days
$t_{1/2}$ = 244 days
IgG
n=222
n=51
IgG AU/ml
D
$t_{1/2}$ = 148 days
$t_{1/2}$ = 324 days
E
$t_{1/2}$ = 157 days
$t_{1/2}$ = 385 days
F
$t_{1/2}$ = 159 days
$t_{1/2}$ = 284 days
IgA
n=190
n=51
IgA AU/ml
G
$t_{1/2}$ = 65 days
$t_{1/2}$ = 98 days
H
$t_{1/2}$ = 66 days
$t_{1/2}$ = 105 days
I
IgM
n=190
n=51
IgM AU/ml
1e+06
1e+04
1e+02
0
50
100
150
200
250
Days since symptom onset
COVID-19
Pre-pandemic
Exponential
Power Law

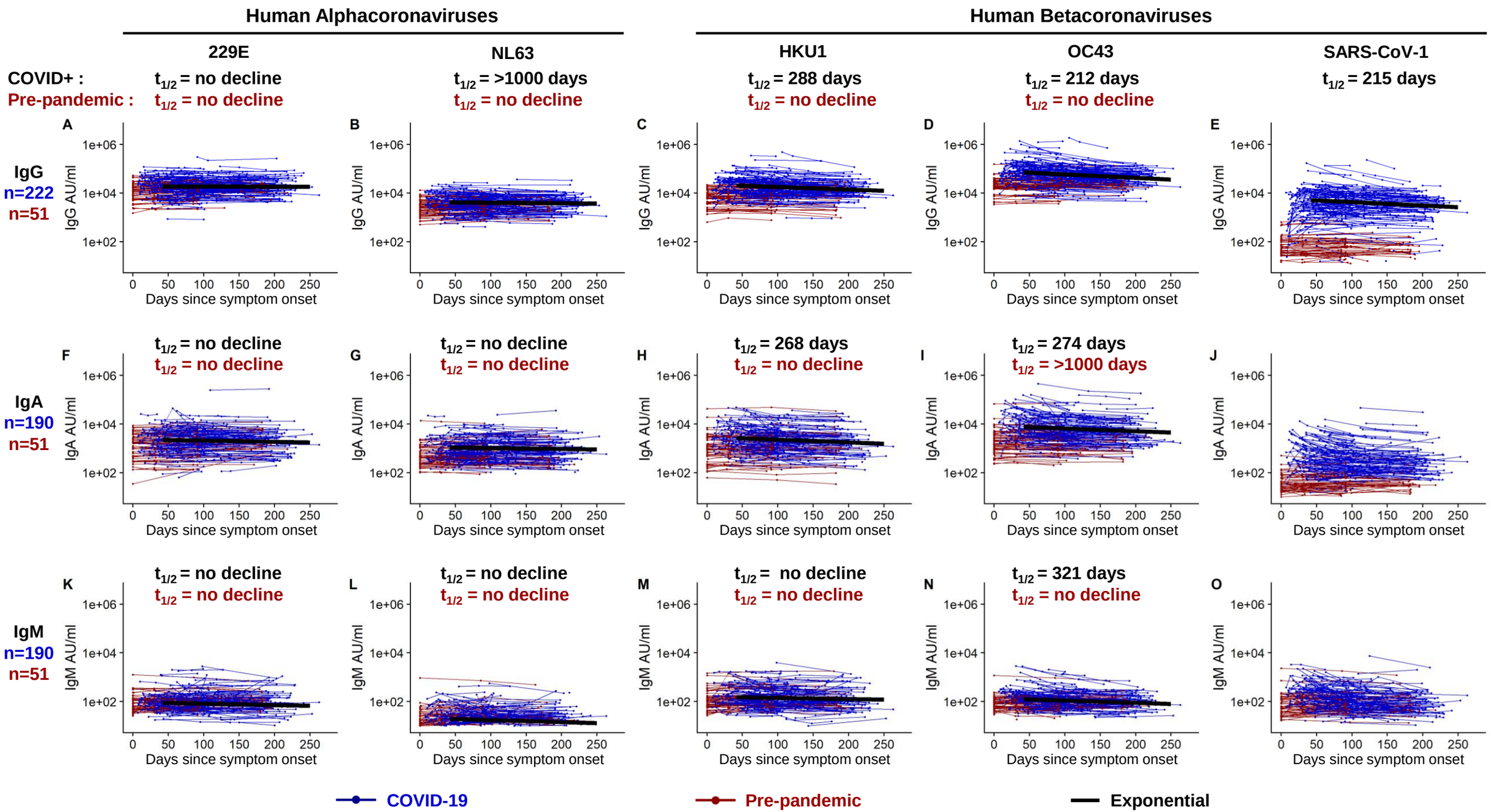
Human Alphacoronaviruses
Human Betacoronaviruses
229E
NL63
HKU1
OC43
SARS-CoV-1
COVID+ :
Pre-pandemic :
t1/2 = no decline
t1/2 = no decline
t1/2 = >1000 days
t1/2 = no decline
t1/2 = 288 days
t1/2 = no decline
t1/2 = 212 days
t1/2 = no decline
t1/2 = 215 days
IgG
n=222
n=51
IgA
n=190
n=51
IgM
n=190
n=51
t1/2 = no decline
t1/2 = no decline
t1/2 = no decline
t1/2 = no decline
t1/2 = 268 days
t1/2 = no decline
t1/2 = 274 days
t1/2 = >1000 days
t1/2 = no decline
t1/2 = no decline
t1/2 = no decline
t1/2 = no decline
t1/2 = no decline
t1/2 = 321 days
t1/2 = no decline
IgG AU/ml
IgA AU/ml
IgM AU/ml
1e+06
1e+04
1e+02
0 50 100 150 200 250
Days since symptom onset
COVID-19
Pre-pandemic
Exponential

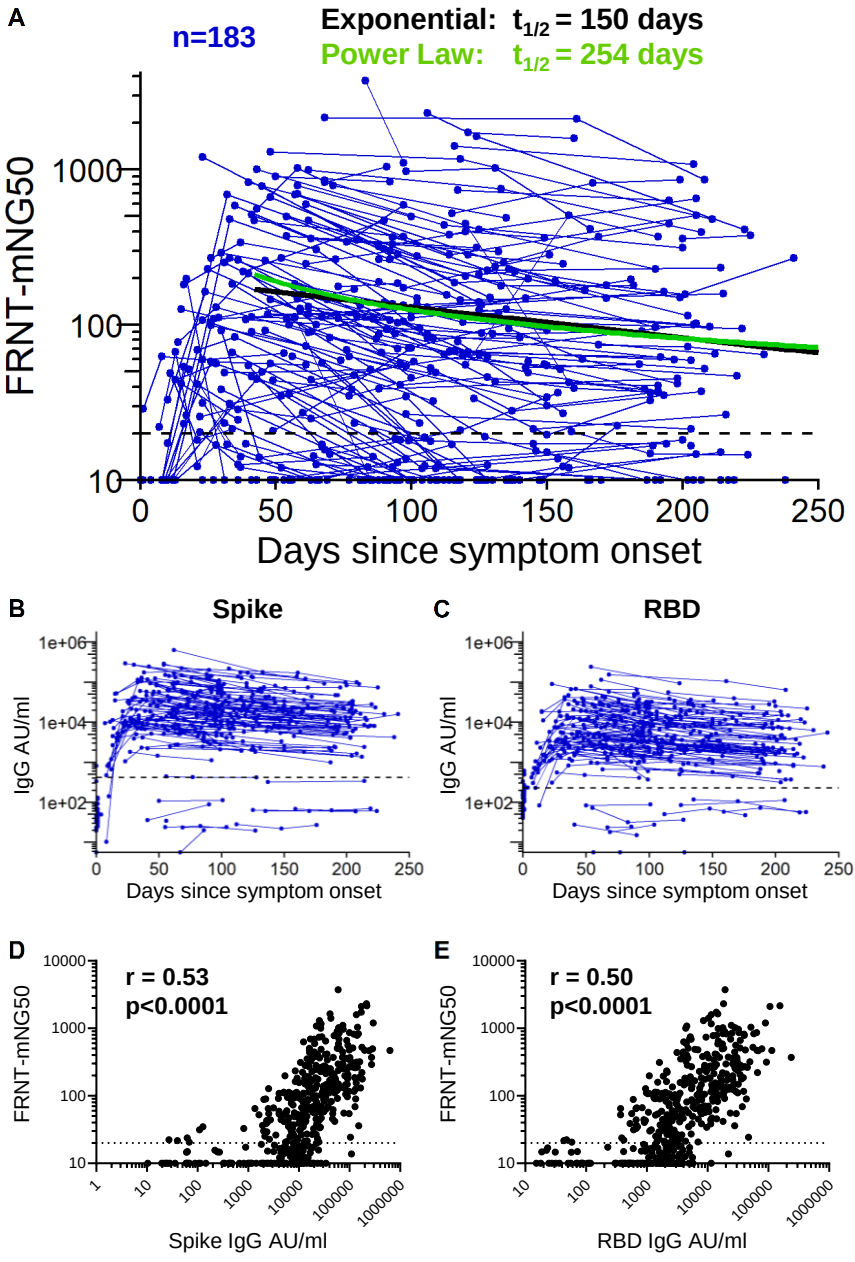
A
n=183
Exponential: $t_{1/2}$ = 150 days
Power Law: $t_{1/2}$ = 254 days
FRNT-mNG50
1000
100
10
0
50
100
150
200
250
Days since symptom onset
B
Spike
IgG AU/ml
1e+06
1e+04
1e+02
Days since symptom onset
C
RBD
IgG AU/ml
1e+06
1e+04
1e+02
Days since symptom onset
D
r = 0.53
p<0.0001
FRNT-mNG50
10000
1000
100
10
1
Spike IgG AU/ml
1000000
E
r = 0.50
p<0.0001
FRNT-mNG50
RBD IgG AU/ml

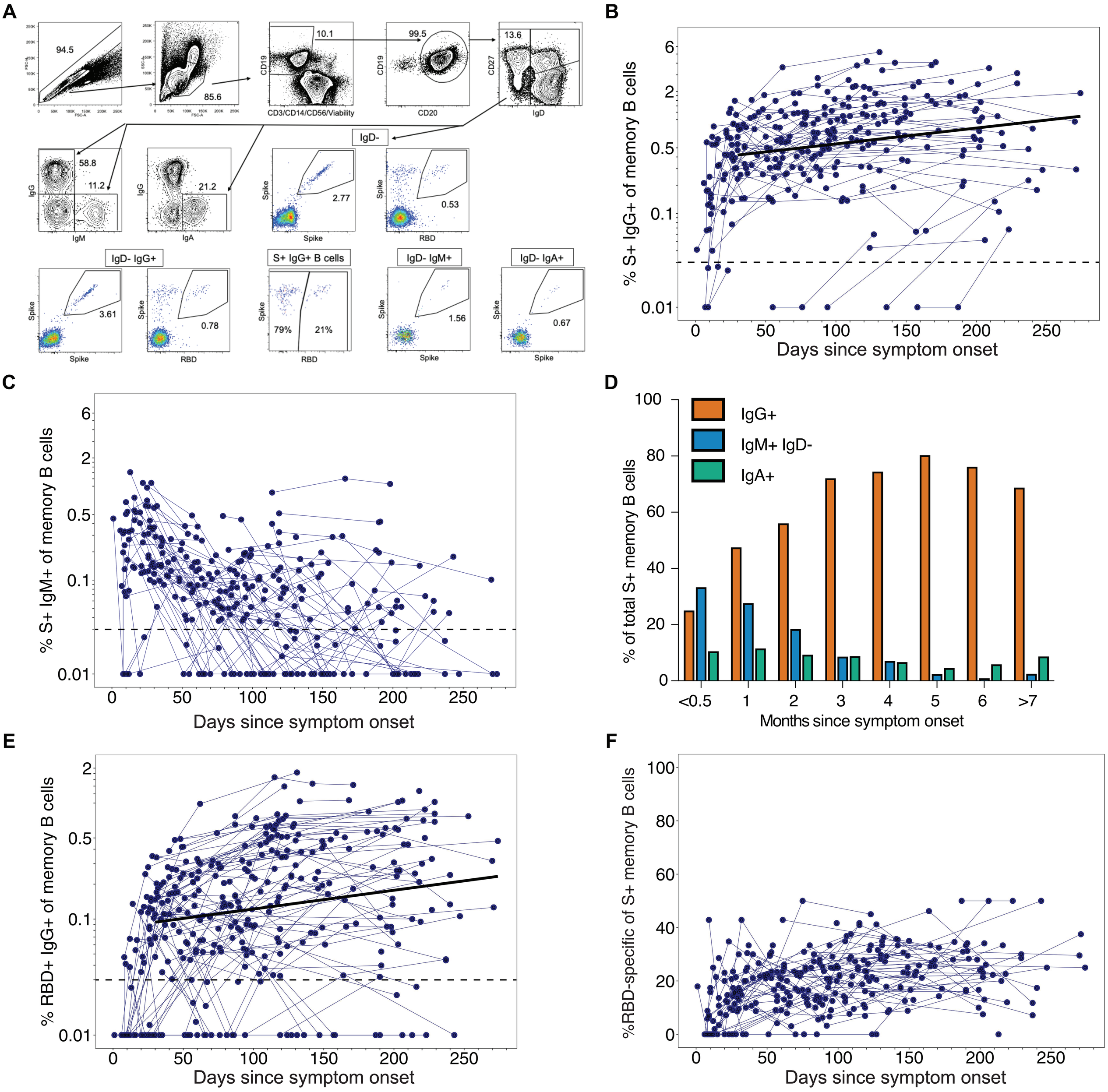
A
94.5
85.6
10.1
99.5
13.6
CD19
CD3/CD14/CD56/Viability
CD20
CD27
IgD
IgD-
58.8
11.2
21.2
2.77
0.53
IgG
IgM
IgA
Spike
RBD
IgD- IgG+
S+ IgG+ B cells
IgD- IgM+
IgD- IgA+
3.61
0.78
79%
21%
1.56
0.67
B
% S+ IgG+ of memory B cells
Days since symptom onset
C
% S+ IgM+ of memory B cells
Days since symptom onset
D
IgG+
IgM+ IgD-
IgA+
% of total S+ memory B cells
<0.5
1
2
3
4
5
6
>7
Months since symptom onset
E
% RBD+ IgG+ of memory B cells
Days since symptom onset
F
%RBD-specific of S+ memory B cells
Days since symptom onset

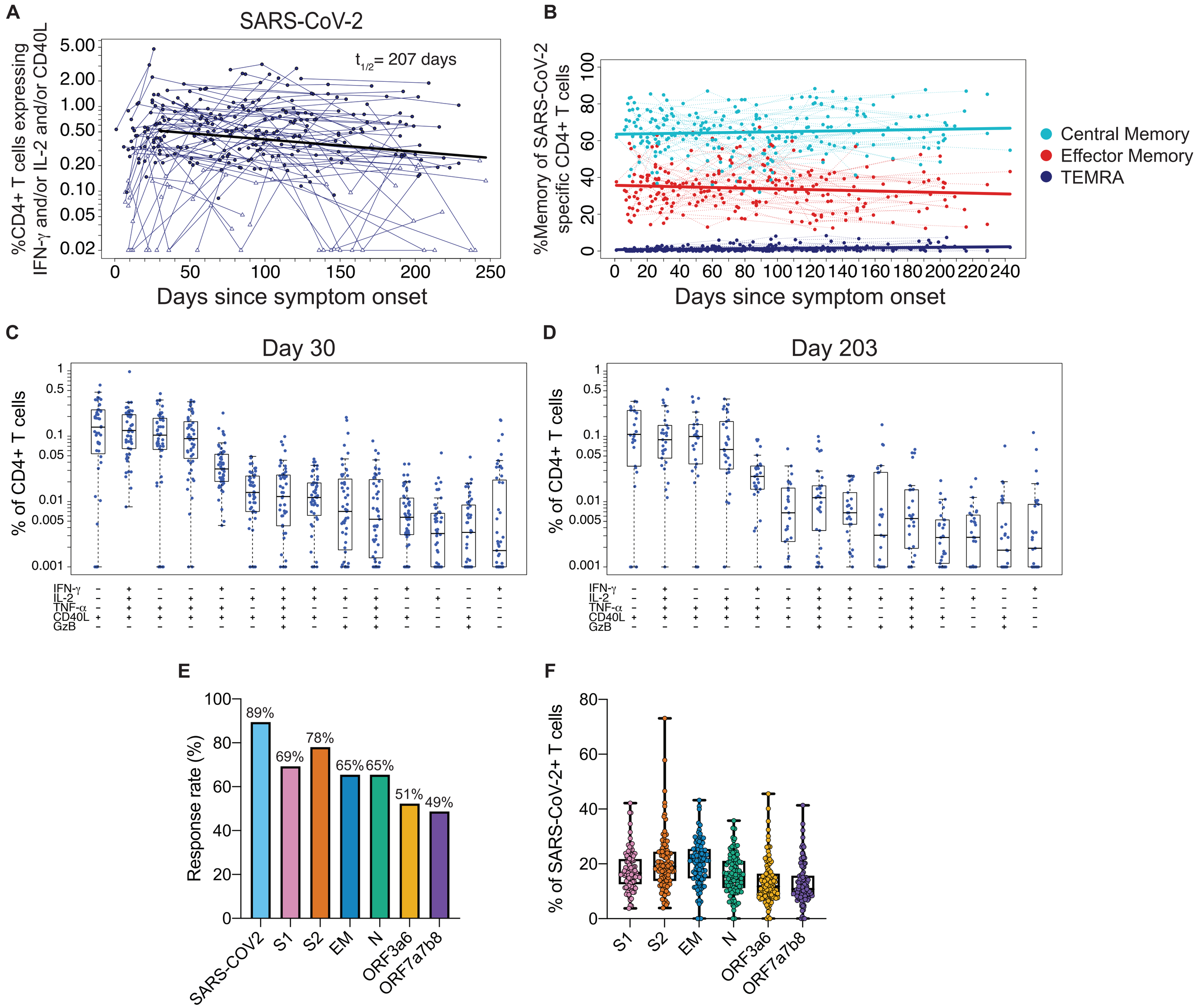
A
SARS-CoV-2
$t_{1/2}$= 207 days
%CD4+ T cells expressing IFN-γ and/or IL-2 and/or CD40L
Days since symptom onset
B
%Memory of SARS-CoV-2 specific CD4+ T cells
Days since symptom onset
Central Memory
Effector Memory
TEMRA
C
Day 30
% of CD4+ T cells
IFN-γ
IL-2
TNF-α
CD40L
GzB
D
Day 203
% of CD4+ T cells
E
Response rate (%)
89%
69%
78%
65%
65%
51%
49%
SARS-COV2
S1
S2
EM
N
ORF3a6
ORF7a7b8
F
% of SARS-CoV-2+ T cells
S1
S2
EM
N
ORF3a6
ORF7a7b8

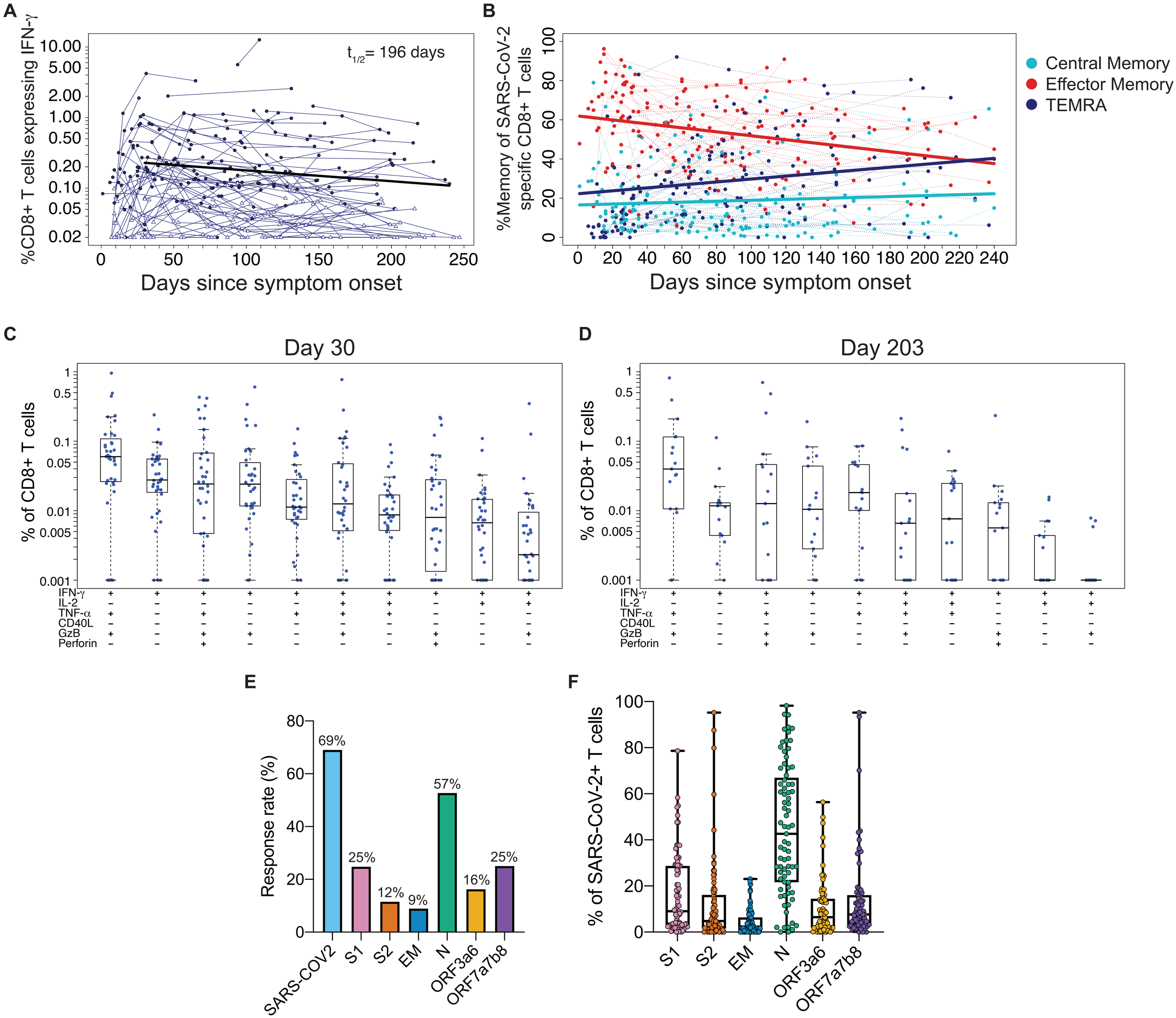
A
%CD8+ T cells expressing IFN-γ
10.00
5.00
2.00
1.00
0.50
0.20
0.10
0.05
0.02
t1/2= 196 days
0
50
100
150
200
250
Days since symptom onset
B
%Memory of SARS-CoV-2 specific CD8+ T cells
0
20
40
60
80
100
0 20 40 60 80 100 120 140 160 180 200 220 240
Days since symptom onset
Central Memory
Effector Memory
TEMRA
C
Day 30
% of CD8+ T cells
1
0.5
0.1
0.05
0.01
0.005
0.001
IFN-γ
IL-2
TNF-α
CD40L
GzB
Perforin
D
Day 203
% of CD8+ T cells
E
Response rate (%)
80
60
40
20
0
69%
25%
12%
9%
57%
16%
25%
SARS-COV2
S1
S2
EM
N
ORF3a6
ORF7a7b8
F
% of SARS-CoV-2+ T cells
100
80
60
40
20
0
S1
S2
EM
N
ORF3a6
ORF7a7b8

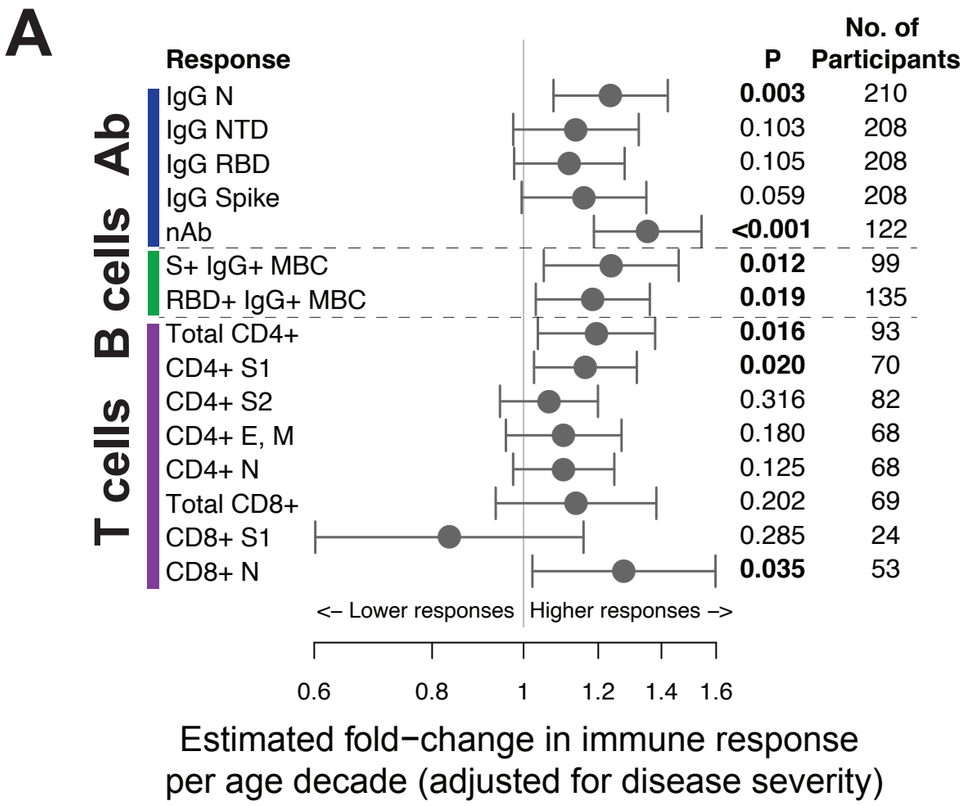
A
Response
P
No. of Participants
Ab
B cells
T cells
IgG N 0.003 210
IgG NTD 0.103 208
IgG RBD 0.105 208
IgG Spike 0.059 208
nAb <0.001 122
S+ IgG+ MBC 0.012 99
RBD+ IgG+ MBC 0.019 135
Total CD4+ 0.016 93
CD4+ S1 0.020 70
CD4+ S2 0.316 82
CD4+ E, M 0.180 68
CD4+ N 0.125 68
Total CD8+ 0.202 69
CD8+ S1 0.285 24
CD8+ N 0.035 53
<– Lower responses
Higher responses –>
0.6 0.8 1 1.2 1.4 1.6
Estimated fold−change in immune response
per age decade (adjusted for disease severity)

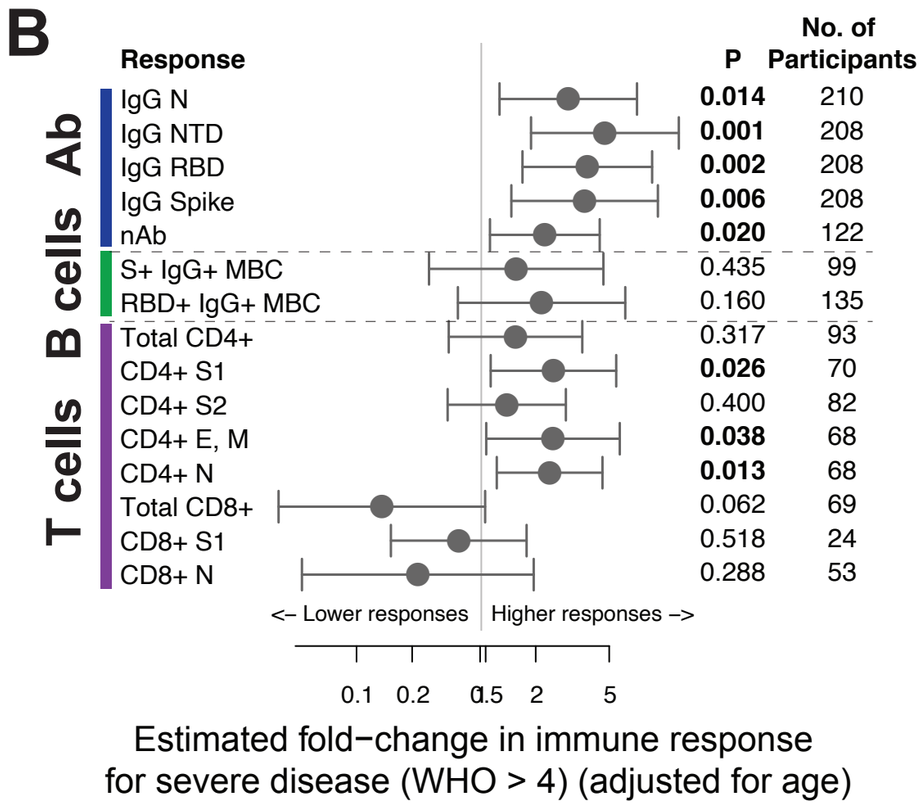
B
Response
P
No. of Participants
Ab
B cells
T cells
IgG N 0.014 210
IgG NTD 0.001 208
IgG RBD 0.002 208
IgG Spike 0.006 208
nAb 0.020 122
S+ IgG+ MBC 0.435 99
RBD+ IgG+ MBC 0.160 135
Total CD4+ 0.317 93
CD4+ S1 0.026 70
CD4+ S2 0.400 82
CD4+ E, M 0.038 68
CD4+ N 0.013 68
Total CD8+ 0.062 69
CD8+ S1 0.518 24
CD8+ N 0.288 53
<– Lower responses
Higher responses –>
0.1 0.2 0.5 1 2 5
Estimated fold−change in immune response
for severe disease (WHO > 4) (adjusted for age)

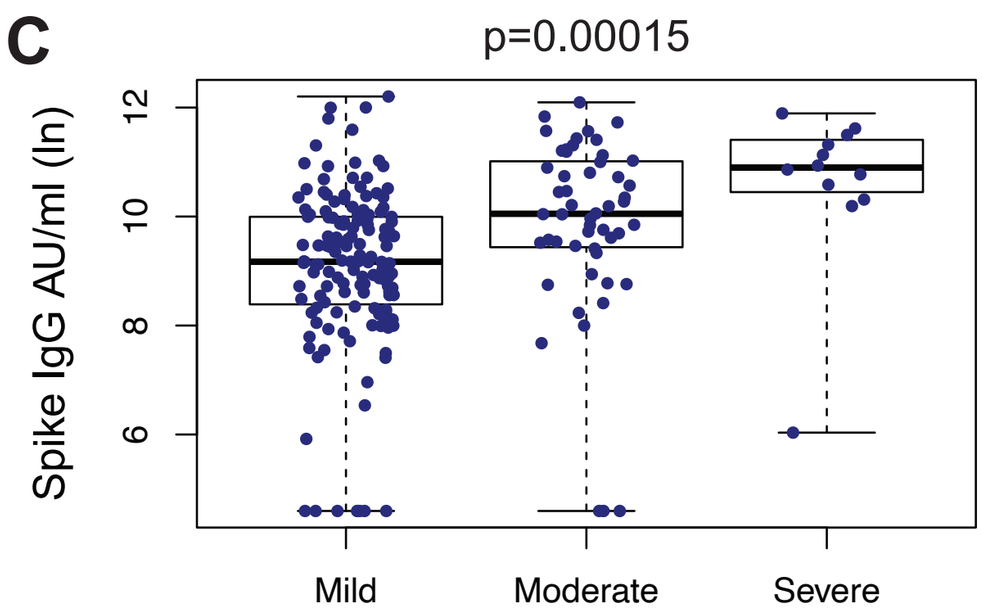
C
p=0.00015
Spike IgG AU/ml (ln)
6 8 10 12
Mild
Moderate
Severe

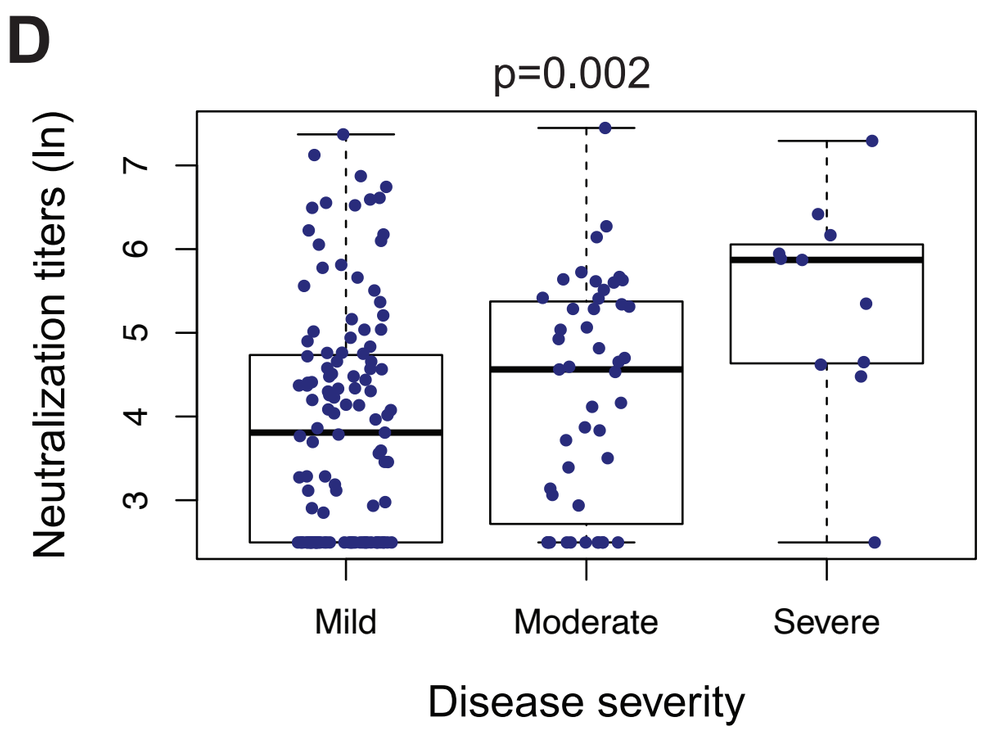
D
p=0.002
Neutralization titers (ln)
3 4 5 6 7
Mild
Moderate
Severe
Disease severity

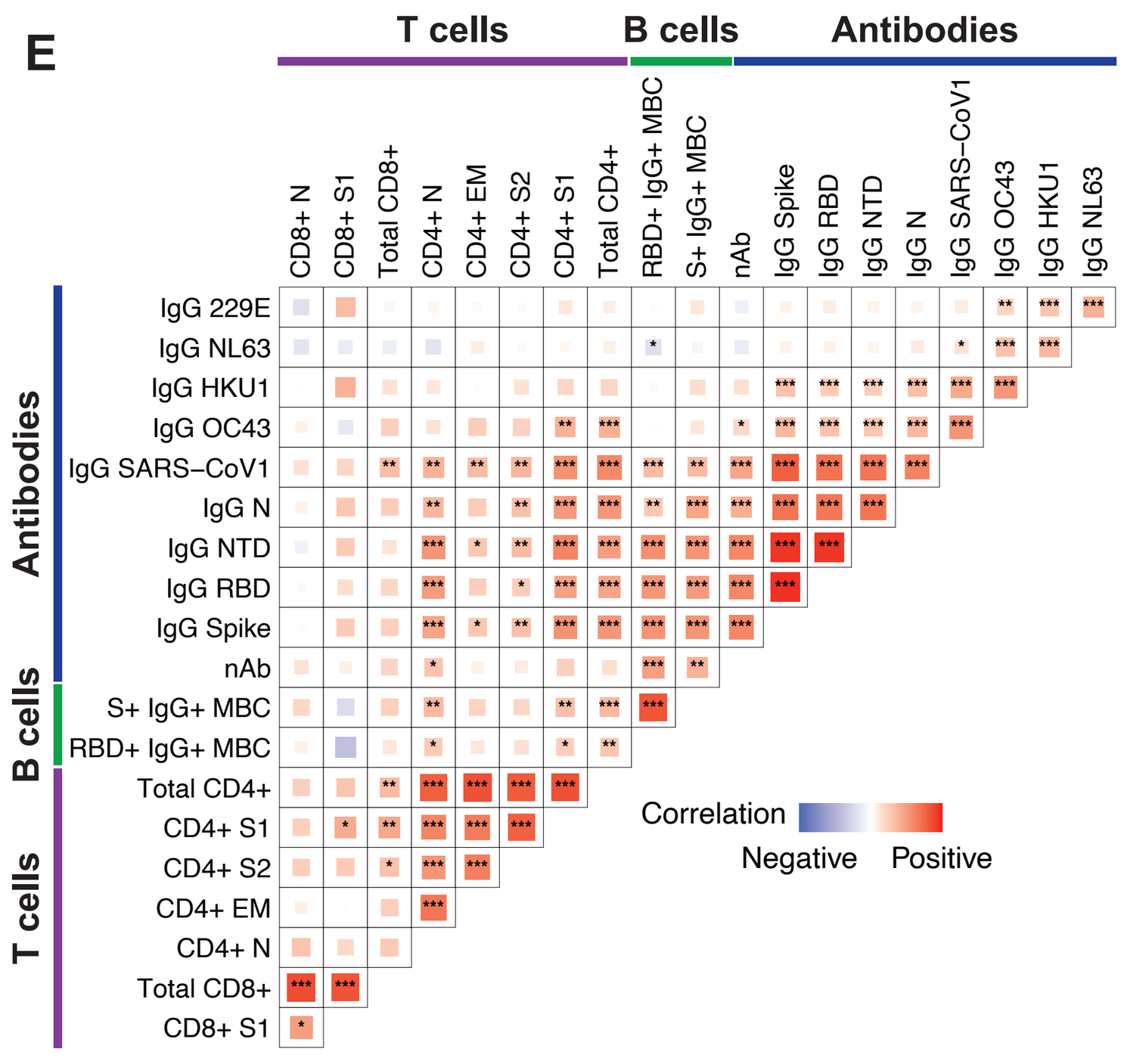
E
T cells
B cells
Antibodies
CD8+ N
CD8+ S1
Total CD8+
CD4+ N
CD4+ EM
CD4+ S2
CD4+ S1
Total CD4+
RBD+ IgG+ MBC
S+ IgG+ MBC
nAb
IgG Spike
IgG RBD
IgG NTD
IgG N
IgG SARS−CoV1
IgG OC43
IgG HKU1
IgG NL63
IgG 229E
Antibodies
B cells
T cells
Correlation
Negative
Positive